An A-train and model perspective on the vertical distribution of aerosols and CO in the Northern Hemisphere

Bonne Ford[1] and Colette L. Heald[1,2]

Received 5 October 2011; revised 18 January 2012; accepted 30 January 2012; published 27 March 2012.

[1] We use A-train satellite observations of aerosols and carbon monoxide (CO) (CALIOP, MODIS, and TES) with GEOS-Chem model simulations to analyze long range transport in the Northern Hemisphere over 3 years (December 2006–November 2009), with a focus on the vertical distribution of pollutants. GEOS-Chem underestimates TES observations of CO in all seasons (<25%) except winter. MODIS and GEOS-Chem aerosol optical depths (AOD) are both generally biased high in comparison with CALIOP (0.042 over land/0.036 over ocean and 0.016 over land/−0.0071 over ocean, respectively; for spring seasons, but similar results for all seasons). Comparisons between GEOS-Chem and CALIOP improve when the CALIOP detection limits are accounted for, and the bias over land in particular is reduced (0.010). However, we find that GEOS-Chem with applied detection limits still overestimates the CALIOP observations of aerosol extinction over sources in Asia and Europe, but underestimates in marine environments and over North America in spring and summer. Vertical cross-sections indicate that GEOS-Chem may be removing aerosol too efficiently in the boundary layer in addition to underestimating marine aerosol sources. We show that mimicking the single aerosol type per layer retrieval of CALIOP with GEOS-Chem could lower simulated AOD by 10–30% at midlatitudes. TES and CALIOP observations confirm that while CO is efficiently transported aloft (only 12% of the CO column is within the planetary boundary layer (PBL) on average), the efficient removal of aerosol limits export and subsequent transport with over 50% of observed aerosol extinction occurring within the PBL.

Citation: Ford, B., and C. L. Heald (2012), An A-train and model perspective on the vertical distribution of aerosols and CO in the Northern Hemisphere, *J. Geophys. Res.*, *117*, D06211, doi:10.1029/2011JD016977.

1. Introduction

[2] The detrimental effects of atmospheric pollution on human health, agriculture, and visibility motivate many countries to set stringent air quality regulations. Although local emissions are the main cause of air quality degradation, episodic long range transport (LRT) can also contribute to elevated pollutant concentrations [e.g., *Li et al.*, 2002; *Parrish et al.*, 2009]. The vertical distribution of pollutants is a key factor in transport efficiency and the ultimate impact on downwind air quality. In this study our objective is to use satellite observations to investigate the vertical structure of pollution during export and long range transport. We focus on the Northern Hemisphere midlatitudes as a highly populated region with significant anthropogenic emission sources, making LRT a more frequent and potent problem than in the Southern Hemisphere. Specifically, we examine export and transport out of three main regions: Asia, Europe, and North America.

[3] Pollution exported from these regions follows distinct pathways. North American gas and particulate pollutants are primarily transported by warm conveyor belts northeast toward Europe with a smaller percentage transported as far as eastern Russia [*Li et al.*, 2005]. Asian emissions are also transported to the northeast and have the greatest impact on the western coast of North America in the springtime [*Stohl et al.*, 2002; *Yu et al.*, 2008]. Export from Europe has three distinct transport pathways as noted by *Duncan and Bey* [2004] with the most dominant export toward the northeast over Russia, which can also lead to transport to the Arctic, where it is notably the cause of Arctic haze [*Quinn et al.*, 2007; *Stohl et al.*, 2002]. There is also transport westward over the North Atlantic, across the Mediterranean Sea toward North Africa, and eastward to Asia [e.g., *Chin et al.*, 2007]; however, these pathways track over regions with significant local emissions and are therefore harder to distinguish from observations.

[4] Although there is evidence for the long range transport of many atmospheric constituents, most research has focused on regulated species such as PM [*Prospero*, 1981; *Jaffe et al.*, 1999; *Akimoto*, 2003; *Duncan and Bey*, 2004; *Heald et al.*, 2006; *Quinn et al.*, 2007; *Ansmann et al.*, 2009; *Reidmiller*

[1]Department of Atmospheric Science, Colorado State University, Fort Collins, Colorado, USA.
[2]Now at Department of Civil and Environmental Engineering, MIT, Cambridge, Massachusetts, USA.

0148-0227/12/2011JD016977

et al., 2009], ozone [*Derwent et al.*, 2004; *Guerova et al.*, 2006] and its precursors. The effectiveness of long range transport of these pollutants from source regions to downwind receptor sites is determined by several factors: the initial amount emitted, the lifetime of the species against transformation and removal, the contribution from en-route production, the transport pathway, and transport efficiency (how quickly a pollutant is transported with respect to its lifetime). Transport can occur at low altitudes through boundary layer ventilation or advection with the mean winds, but these processes generally take place on timescales of days to weeks, and therefore are inefficient for chemical species with shorter lifetimes [*Dacre et al.*, 2007; *Keating and Zuber*, 2007]. The lifetime of ozone and PM can be extended when lofted into the colder free troposphere [*Keating and Zuber*, 2007]. Furthermore, since winds generally strengthen with height, these species can be transported more rapidly aloft. Therefore, for more efficient transport, pollutants must first be vertically lofted out of the boundary layer and into the upper troposphere through strong convection, warm conveyor belts, turbulent mixing, or orographic lifting [*Liu et al.*, 2003].

[5] Given the efficiency of transport in the free troposphere, many LRT events are detected at elevated sites such as the Mount Bachelor Observatory [*Reidmiller et al.*, 2009] or the PICO-NARE station on Pico mountain [*Owen et al.*, 2006]. Clean background air sampled at these sites also facilitates the identification of transported plumes. While transport is more efficient in the free troposphere; if plumes remain aloft, they have little direct impact on lower altitude surface sites downwind (although wet removal may still lead to surface deposition and the associated radiative impacts can modify photolysis rates [*Jacobson*, 1998; *Liao et al.*, 1999]). The efficiency of descent, via subsidence or mountain circulations, ultimately determines the magnitude of the disturbance or contribution to background surface concentrations. However, detecting an observable influence of LRT at the surface is complicated by local influences and the dilution of plumes during descent [*Hudman et al.*, 2004; *Heald et al.*, 2006].

[6] Identification of LRT plumes is also complicated by the fact that long range transport often occurs over ocean basins or remote continental regions where in situ observations are limited. Assessing LRT impacts has therefore relied on interpreting the observational record at a receptor region [e.g., *Prospero*, 1999; *Jaffe et al.*, 1999] or at an island site located between source and receptor [*Levy and Moxim*, 1989; *Perry et al.*, 1999] with little information on the processes or pathway during transport. Aircraft data from field campaigns provide useful information about the vertical distribution and specific in-plume processing of pollutants, as aircraft are able to follow plume progression and sample the same plume multiple times, but like surface observations, these campaigns suffer from spatial and/or temporal constraints [*Heald et al.*, 2004; *Hudman et al.*, 2004; *Price et al.*, 2004; *Fehsenfeld et al.*, 2006; *Singh et al.*, 2006; *Fuelberg et al.*, 2010]. While satellite observations offer the possibility of continuous global coverage, due to poor vertical resolution, satellites have been primarily used to track the spatial progression of plumes [*Edwards et al.*, 2004; *Heald et al.*, 2004, 2006; *Yu et al.*, 2008]. Ultimately, this lack of information on the vertical distribution makes it more difficult to translate these satellite observations into surface concentrations and determine the impact on air quality at downwind sites [*Al-Saadi et al.*, 2005; *van Donkelaar et al.*, 2010].

[7] The implementation of improved satellite technology with heightened vertical resolution therefore provides the opportunity to better examine the export and long range transport of pollutants. The CALIOP instrument, a space-based lidar, provides an unprecedented look at the vertical distribution of clouds and aerosols in the global atmosphere [*Winker et al.*, 2010]. Because carbon monoxide (CO) has strong absorption lines in the thermal infrared (IR) and solar shortwave IR, which are observable from space; by using calibrated measurements of CO radiance, instruments such as TES are able to retrieve some vertical information on the distribution of CO [*Deeter et al.*, 2004].

[8] In this study, we use A-train observations, including CALIOP aerosol extinction, Aqua MODIS aerosol optical depths (AOD) and TES CO, to study long range transport in the Northern Hemisphere. In particular, we use these observations to test the vertical representation of transport processes in the global chemical transport model GEOS-Chem. Carbon monoxide is used here as a contrast to aerosol, whose shorter lifetime and higher solubility suggest different transport pathways [*Heald et al.*, 2006]. We use the GEOS-Chem model to interpret these observations and to identify contributions due to differing sources and species at receptor sites.

2. Descriptions of Observation and Modeling Tools

2.1. CALIOP Aerosol Extinction

[9] The Cloud-Aerosol Lidar with Orthogonal Polarization (CALIOP) was launched aboard the Cloud-Aerosol Lidar and Infrared Pathfinder Satellite Observations (CALIPSO) satellite on April 28, 2006 as part of the A-train constellation. CALIOP measures the backscatter intensity and the orthogonally polarized components of the backscatter signal at two wavelengths, 532 nm and 1064 nm with a 30 m vertical resolution in the troposphere [*Winker et al.*, 2003]. CALIPSO takes 16 days to repeat its orbit; so with a ~100 m footprint, full global coverage for CALIPSO also takes approximately 16 days [*Hunt et al.*, 2009].

[10] Details of the data processing algorithms for CALIOP are given by *Winker et al.* [2009] and of the aerosol classification by *Omar et al.* [2009]. In brief, level 1 processing involves geolocation and calibration, while the level 2 algorithm is a multistep process which first identifies cloud and aerosol layers, then uses a set of scene classification algorithms (SCA) to determine the layer type (cloud or aerosol and then aerosol type or cloud ice-water phase), and then backscatter and extinction coefficient profiles are retrieved. This retrieval requires a lidar ratio in order to convert backscatter to extinction. This value can be derived from layer transmittance (if a distinct layer is surrounded by clear air) or specified as a predetermined value based on the SCA, which occurs most commonly. Six aerosol types are used as shown in Table 1 (defined from cluster analysis of AERONET data sets [*Dubovik and King*, 2000]) and are determined using the two wavelength backscatter measurements, volume depolarization ratios, surface type, geographic location and layer altitude (*Omar et al.* [2009] gives flowchart of selection

Table 1. CALIOP Aerosol Types and Associated Lidar Ratios for 532 nm Wavelength[a]

Aerosol Type	Lidar Ratio
Dust	40 sr
Polluted Dust	60 sr
Smoke	70 sr
Polluted Continental	70 sr
Clean Continental	35 sr
Clean Marine	20 sr

[a]From *Winker et al.* [2009].

scheme). Therefore the selection criteria can strongly affect the retrieved extinction profiles, and even more so, the spatial and vertical distributions of tropospheric aerosol types in CALIOP data. For example, over snow or ice, observed aerosols can only be classified as clean or polluted continental but never dust [*Omar et al.*, 2009], even though transport of Asian dust and smoke to the Arctic has been observationally noted [e.g., *Barrie and Barrie*, 1990]. *Mielonen et al.* [2009] compared CALIOP aerosol types with AERONET aerosol sites and found that they were in general good agreement (70%), with best agreement for dust containing air masses. It is important to consider these constraints and acknowledge that if aerosols are being misclassified in the retrieval, the wrong lidar ratio might also be applied and could therefore bias the vertical extinction profiles shown in the following sections [*Yu et al.*, 2010; *Oo and Holz*, 2011]. When we consider the differences in selected lidar ratios (Table 1), it is evident that certain regions might be more prone to biases, such as off Africa or Asia when distinguishing between dust and pollution or smoke, or in outflow regions distinguishing between clean marine or pollution, where differences in lidar ratios for these aerosol types are large. We discuss this further in sections 4 and 5.

[11] For aerosol extinction data, we use the CALIPSO Lidar Level 2 Version 3.01 5-km Aerosol Profiles for three years (December 2006 through November 2009) and filter the data using cloud aerosol distinction (CAD) scores, extinction uncertainty values, atmospheric volume descriptors, extinction quality control (QC) flags and total column optical depths. CAD scores are a numerical measure of the confidence of the algorithm classification of observed layers, with negative values used for aerosols and positive values for clouds [*Liu et al.*, 2004]. Therefore, we discard any observations with absolute values below 20, which is a more relaxed criterion than *Yu et al.* [2010] suggests, but allows for a greater sample volume. *Liu et al.* [2009] and *Yu et al.* [2010] both note that thick aerosol layers near source regions are often misclassified by the CAD algorithm, which could lead to some low bias in our analysis of CALIOP data near sources. We also choose to use only clear sky columns by discarding any columns with cloud optical depths greater than zero. Additionally, since CALIOP cannot make observations below thick aerosol layers, we omit any columns with aerosol optical depths greater than two, although this can, in some circumstances, eliminate heavy aerosol events. Extinction uncertainty values and quality control flags are used to remove any observation where the extinction calculation failed or produced non-physical results. We make the approximation that all extinction observations with a corresponding atmospheric volume descriptor that indicates clear air have zero aerosol extinction (rather than the fill value of −9999). We choose to assign a value of zero rather than a value related to the detection limit because the detection limit is for backscatter, and since we use extinction profiles for this work, is dependent on aerosol type (discussed further in section 4 and subsequent sections). For the night (day) observations, this filtering eliminates ∼17% (12%) of the extinction values and makes ∼77% (84%) of the profile extinction values 0 (indicating that most of the profile is "clear air").

[12] CALIPSO has an ascending equator crossing at 1330 local solar time (LST) and a descending node at 0130 LST. *Kittaka et al.* [2010] show that CALIOP AOD distributions derived from the earlier Level 2 Version 2.01 layer products are similar for day and night. For this work, except for comparison with MODIS and when discussing fractions in the planetary boundary layer (PBL), we choose to use the nighttime data because the signal-to-noise ratio (SNR) is greater during the night due to the lack of noise from background solar illumination [*Hunt et al.*, 2009]. Comparisons of seasonally averaged AOD from CALIOP show that daytime observations have a slight low bias (generally less than 20%) compared to the night observations in source and outflow regions, and a slight high bias over remote marine regions (generally less than 5%).

2.2. Aqua MODIS Aerosol Optical Depth

[13] The Moderate-resolution Imaging Spectroradiometer (MODIS) measures scattered radiances at 36 wavelengths and provides almost daily global coverage of AOD observations in the absence of clouds. Two different algorithms are used for AOD retrievals over the ocean and the land to account for the contribution of surface reflectance. Although AOD is only retrieved over dark land surfaces [*Kaufman et al.*, 1997], the use of an estimated surface reflectance has been shown to produce a high bias over bright land surfaces [*Drury et al.*, 2010]. Numerous studies have evaluated MODIS AOD (τ) through comparisons with ground based AERONET stations and have shown generally good agreement with expected uncertainties in the MODIS-derived AOD of $\pm$ 0.03 $\pm$ 0.05 τ over ocean and $\pm$ 0.05 $\pm$ 0.15 τ over land [*Remer et al.*, 2008; *Levy et al.*, 2010].

[14] For this work, we use data from MODIS aboard the Aqua platform which flies in the A-train constellation, one minute and fifteen second ahead of CALIPSO. Specifically, we use Collection 5, Level 3 daily files, which are on a 1° by 1° grid. We combine land and ocean optical depth retrievals, and filter the data to include only grid boxes with (cloud mask) cloud fractions below 0.8 and aerosol optical depths less than 1.5 following *Zhang and Reid* [2006]. *Redemann et al.* [2011] note that using only scenes with a MODIS cloud fraction of 1% or less generally improves correlations between MODIS and CALIOP (also used by *Oo and Holz* [2011]), compared with the 80% cut-off employed here. However, this would remove a significant percent of observations.

2.3. TES Carbon Monoxide

[15] We use observations of CO from the Tropospheric Emission Spectrometer (TES), which is one of four instruments

aboard the NASA Earth Observing System (EOS) Aura platform. Aura was launched on July 15, 2004 into the A-train formation, flying eight minutes behind Aqua. TES is an infrared, high-resolution Fourier transform spectrometer. Global surveys are made roughly every other day, and with a spatial coverage of 5.3 km by 8.5 km in the nadir (and approximately 180 km between successive nadir observations), a full global survey requires approximately 16 days or 233 orbits [*Beer et al.*, 2001].

[16] The retrieval algorithm for TES uses the optimal estimation approach as described by *Rodgers* [2000]. The retrieved CO volume mixing ratio ($\hat{\mathbf{x}}$) is expressed as the linear combination of the true profile weighted by the averaging kernel ($\mathbf{A}$) and the a priori profile ($\mathbf{x_a}$), along with the spectral measurement error ($\boldsymbol{\varepsilon}$).

$$\ln \hat{x} = \ln x_a + A(\ln x - \ln x_a) + \varepsilon \quad (1)$$

[17] The averaging kernel is a measure of the sensitivity of the retrieval to the true state of the atmosphere, and its trace, also known as the degrees of freedom (DOF), tells how many statistically independent elements of information were available from the measurements to calculate the profile. Full TES CO profiles generally have 1–1.5 pieces of information in the troposphere [*Luo et al.*, 2007a, 2007b; *Parrington et al.*, 2008] (these studies also provide further discussion and examples of TES averaging kernels). Retrieved profiles with low DOFs are dominated at most levels by the a priori profile, which is generated from MOZART CTM output of monthly mean mixing ratios averaged over 10° latitude by 60° longitude bins.

[18] For this work, we are using Level 2, Version 004 Global Survey nadir observations of CO for December 2006 through November 2009. We use daytime observations because of the heightened vertical resolution in the lower troposphere due to increased thermal contrast [*Deeter et al.*, 2007]. We also filter the data using the recommended ranges for Quality Flags for CO [*Osterman*, 2007]. Figure 1 shows seasonal averages of the total DOFs in the troposphere (up to ~200 hPa) and in the PBL alone. TES profiles generally have about one DOF in the midlatitudes, with little contribution from CO in the PBL.

[19] Several studies validated TES CO with vertical profiles from aircraft campaigns. *Luo et al.* [2007a] find that on average, the TES CO profile in the middle troposphere is 0–10% lower than the in situ profiles taken near Houston during the INTEX-B 2006 campaign, but within the 10–20% retrieval uncertainty. However, CO profiles near Hawaii and Alaska, regions strongly influenced by long range transport, do not agree as well (bias up to ± 35%). *Lopez et al.* [2008] find that TES CO agrees within 5–10% with profiles from two AVE campaigns (in the TES sensitivity range of approximately 700–200 hPa).

2.4. GEOS-Chem Global Model

[20] GEOS-Chem is a global three-dimensional, chemical transport model (CTM) driven by assimilated meteorological observations from the NASA Goddard Earth Observing System (GMAO). For this work, we use GEOS-Chem version 8-01-04 [http://geos-chem.org] with the native meteorology at 0.5° latitude by 0.67° longitude horizontal resolution reduced to a 2° latitude by 2.5° longitude and 47 vertical levels for computational expediency.

[21] This simulation includes tropospheric ozone-nitrogen oxides-hydrocarbon chemistry coupled with aerosol chemistry through inorganic aerosol formation (sulfate, nitrate, ammonium) [*Park et al.*, 2004], heterogeneous reactions [*Evans and Jacob*, 2005], and effects on photolysis rates [*Martin et al.*, 2003]. Aerosol simulations also include primary carbonaceous aerosols [*Park et al.*, 2003], dust [*Fairlie et al.*, 2007], sea salt [*Alexander et al.*, 2005], and secondary organic aerosols (SOA) [*Chung and Seinfeld*, 2002; *Liao et al.*, 2007]. Aerosols and gases are removed by both wet and dry deposition in the model. The wet deposition scheme includes scavenging in convective updrafts, rainout and washout [*Liu et al.*, 2001], while dry deposition of gases and aerosols is dependent on surface characteristics and meteorological conditions [*Wesely*, 1989; *Wang et al.*, 1998]. Aerosol optical depths (AOD) at 550 nm are calculated from the mass concentration and the extinction efficiency for each aerosol type following *Martin et al.* [2003], with updated aerosol size distributions as described by *Drury et al.* [2010]. We do not attempt to account for differences between the model and satellite assumed aerosol optical properties here.

[22] Anthropogenic emissions rely on several regional inventories, such as CAC for Canada (http://www.ec.gc.ca/pdb/cac/cac_home_e.cfm), BRAVO over Mexico [*Kuhns et al.*, 2003], EMEP over Europe and for ship exhaust [*Vestreng et al.*, 2007], EPA NEI99 over the USA which is also used for biofuel [*Hudman et al.*, 2007, 2008] and the Streets [*Zhang et al.*, 2009] inventory for Asia. Emissions in areas not covered by these regional emission inventories are based on the GEIA inventory [*Benkovitz et al.*, 1996], with emissions of nitrogen oxide (NO_x), CO, and sulfur oxide (SO_x) based on the EDGAR emissions inventory [*Olivier and Berdowski*, 2001; *Olivier et al.*, 2001]. Biogenic VOC emissions are calculated interactively following MEGAN [*Guenther et al.*, 2006]. Global anthropogenic emissions of black and organic carbon follow *Bond et al.* [2004] with the exception of North America, where emissions of these species follow *Cooke et al.* [1999] with the seasonality from *Park et al.* [2003]. Biomass burning and biofuel emissions are specified according to the GFED2 inventory [*van der Werf et al.*, 2006] and *Yevich and Logan* [2003] monthly inventories respectively.

[23] The full, online chemistry simulation was run for three years (December 2006–November 2009) with initialization on December 1, 2006 after an eight-month spin-up simulation. Daily diagnostics are output to coincide with A-train overpass time, averaged from 1 to 2 local time for nighttime and 13–14 local time for daytime overpasses. We re-grid all the satellite data to the standard GEOS-Chem 2° × 2.5° grid and then sample the GEOS-Chem output along the satellite observation track by only using grid boxes with valid observations. For TES, we also linearly interpolate the model profile to the 67 valid TES pressure levels before applying the retrieval operator as in equation (1). For direct comparison with MODIS and CALIOP, we also omit GEOS-Chem columns with AOD greater than 1.5. This removes 0.3% of the available grid points. In dust regions (e.g., the Saharan and Taklamakan deserts), this can reduce the

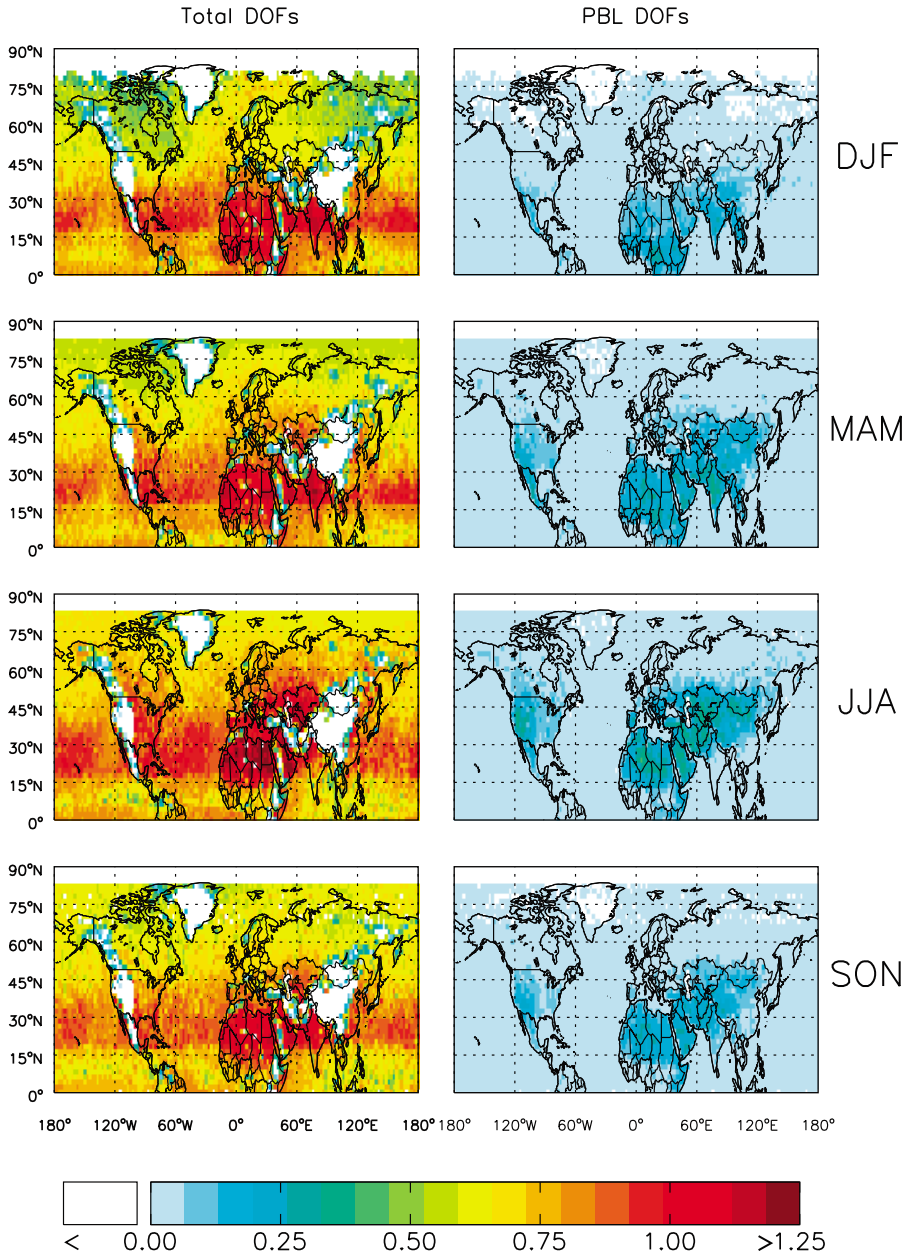

Figure 1. Seasonal averages of the degrees of freedom for TES (left) in the troposphere (up to ~200 hPa) and (right) in the planetary boundary layer. Color bar is saturated at 1.25.

column AOD by 10–60%; however, the global average reduction of AOD is less than 6%.

3. Potential Issues When Comparing GEOS-Chem and Satellite Observations

3.1. Samping Issues

[24] Although model output is matched with observations for comparison; in attempting to examine long range transport events that happen on timescales of several days, the limited spatial coverage of satellites with small footprints such as TES and CALIOP can pose several challenges. While the model may simulate a distinct plume being transported, the satellite may not observe over the region for that day. As shown in Figure 2 for 24 March 2007, GEOS-Chem predicts high AOD values over the North Atlantic due to a plume being transported off the east coast of North America, yet, the CALIOP track for the day misses all but the edges of the plume. On seasonal scales, sampling of the model along the satellite track does not appear to bias the average extinction profile as seen in Figure 2b, which shows that using all model output for spring 2007 over the boxed region in Figure 2a produces an almost identical profile to sampling only when there was a valid satellite observation over the region. However, when we examine the time series of the average AOD for the same region (Figure 2c), several transport events, such as the plume on 24 March 2007, are missed. This implies that comparisons of model simulations with satellite observations with no cross-track scanning (as in CALIOP and TES) can be particularly susceptible to model transport

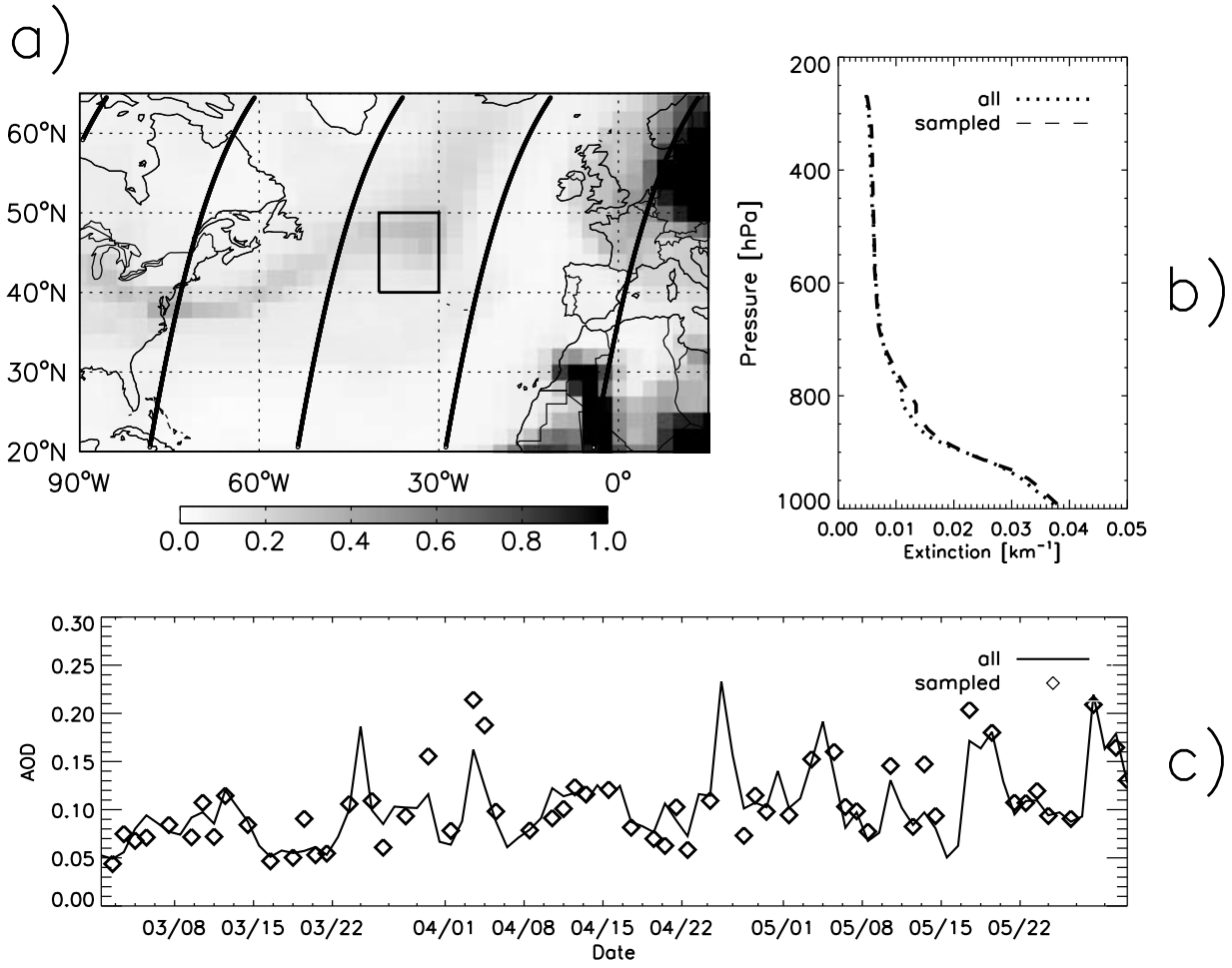

Figure 2. Illustration of satellite sampling issues with no cross-track scanning: (a) AOD from GEOS-Chem with the track for CALIOP (thick black) for 24 March 2007 and the averaging box; (b) average spring 2007 extinction profile within the box indicated in Figure 2a for GEOS-Chem (dotted) and when sampled to the A-train path (dashed); and (c) time series of the mean column AOD in the box indicated in Figure 2a for spring 2007 from GEOS-Chem (solid) and when sampled to the CALIOP overpass (diamonds).

errors. Therefore, while these satellite instruments can provide us with some information on vertical distributions during export and transport events, the small footprints and limited number of valid observations make it difficult to determine broad characteristics about transport in each region from daily observations. Consequently, we choose to analyze LRT as multiyear averages of seasonal timescales in subsequent sections.

3.2. CALIOP Detection Limits

[25] Comparisons between observed and simulated aerosol extinction are also complicated by the CALIOP detection limit. Due to the greater SNR ratio, the detection limit decreases with altitude and during the night [*Winker et al.*, 2009]. Near the surface it is approximately 4–5 $\times$ 10^{-4} km^{-1} sr^{-1} and about 2 $\times$ 10^{-4} km^{-1} sr^{-1} in the middle to upper troposphere [*Winker et al.*, 2009].

[26] Simulated extinction values below the detection limit need to be corrected to 'zeros' to mimic the CALIOP sensitivity and allow for direct comparison. An exact matching of the detection limit can only be done in terms of backscatter, however, this would require application of the CALIOP retrieval algorithm to the simulated backscatter values in order to produce aerosol extinction profiles. This is not trivial. Therefore as a first step toward incorporating the detection limits in our comparisons, we take into account the lidar ratio of each aerosol type (Table 1) noted by *Winker et al.* [2009] and use it to convert the GEOS-Chem simulated aerosol species extinction values into backscatter values and apply a detection limit of 2 $\times$ 10^{-4} km^{-1} sr^{-1}. Extinction values simulated by GEOS-Chem which have a corresponding backscatter value lower than the detection limit are replaced with a value of 0 as they would be observed as "clear air" by CALIOP. The impact of applying detection limits to the GEOS-Chem simulation are shown in sections 4 and 5.

3.3. Results From Previous Studies

[27] In addition to these sampling issues, previous studies note specific biases when comparing GEOS-Chem with these satellites. While MODIS AOD is generally in good spatial agreement with GEOS-Chem, it is biased high over the Pacific, particularly at low loading [*Heald et al.*, 2006], and over land, notably in the western U.S. [*Li et al.*, 2005; *van Donkelaar et al.*, 2010]. This bias is attributed mainly to

application of the land algorithm over varying surface terrains. *Generoso et al.* [2008] compare CALIOP backscatter profiles and AOD from MODIS with GEOS-Chem for dust transport across the Atlantic. They find that model-derived backscatter profiles agree with CALIOP near source but under predict AOD downwind, suggesting either too little transport or too much removal in the model. *Van Donkelaar et al.* [2010] compare GEOS-Chem with version 2 CALIOP relative profiles over various land regions to show that there are similarities in the distribution of AOD and the fraction of AOD in the mixed layer typically differs by less than 5% in the Northern Hemisphere.

[28] Regarding CO, *Kopacz et al.* [2010] find that while GEOS-Chem has higher correlations and fewer differences with TES than MOPITT or AIRS, simulated CO column totals are still biased low over source regions in 2004–2005 in the Northern Hemisphere most likely due to an underestimation of fossil fuel emissions.

[29] We use both newer versions of TES retrievals (v004 versus v002), and of the GEOS-Chem model in our work compared to *Kopacz et al.* [2010]. Their study also includes TES profiles prior to the optical bench warm up in December 2005, which they note substantially improved the quality of the CO data (fourfold increase in signal-to-noise ratio). Finally, our simulations were also performed for different years and using a different meteorological product (GEOS-5 versus GEOS-4, which notably uses different convective parameterizations) from *Kopacz et al.* [2010], thus comparisons shown in Section 4 differ from their previous results.

[30] There are also several studies that note biases between MODIS and CALIOP observed AOD. *Kittaka et al.* [2010] compare daytime cloud-screened AODs from MODIS and an earlier version of CALIOP retrievals for the period June 2006 to August 2008 and find that MODIS AOD is higher than CALIOP over extra-tropical oceans, and that over land, CALIOP AOD is higher at low latitudes and MODIS is higher at midlatitudes. *Redemann et al.* [2011] use version 3 data with stricter data screening and also find that CALIOP is generally biased low. *Oo and Holz* [2011] also note that CALIOP AOD is significantly lower than MODIS over the oceans but attribute this discrepancy to an underestimate in the lidar ratio in the CALIOP algorithm. *Sayer et al.* [2012] calculated lidar ratios from AERONET island sites and suggest that the lidar ratios used for the CALIOP algorithm for marine aerosol are too low by about 50%. We also compare seasonal average AODs from MODIS and CALIOP (further discussion in section 4). Differences between the two can be partially explained by the known biases associated with each instrument and will be discussed in further detail in subsequent sections.

4. Spatial Distribution of Pollutant Transport in the Northern Hemisphere

4.1. Column Concentrations of Aerosols and Carbon Monoxide

[31] Prior to investigating the vertical distribution of pollution transport, we compare the spatial patterns of simulated AOD and CO column with satellite observations to examine the model representation of source regions and transport. Figure 3 compares multiyear seasonal average column CO concentrations from TES and GEOS-Chem (with the TES retrieval operator applied as described in section 2), and highlights that the long lifetime of CO enhances background concentrations hemispherically. Model underestimates in spring and summer are typically less than 25%; overestimates at high Northern latitudes in winter generally do not exceed 20%. Our comparisons here agree with *Kopacz et al.* [2010] except in winter, when GEOS-Chem is generally higher than TES (section 3.3).

[32] Both model and observations identify the major source regions and highlight the seasonality in the atmospheric oxidant loading and emissions. Significant export of CO from Northern Hemisphere source regions is easily identified with the TES observations. GEOS-Chem captures the seasonality of this export and transport (Figure 3); previous studies have demonstrated the model's skill in reproducing specific events observed by TES [*Zhang et al.*, 2008; *Reidmiller et al.*, 2009].

[33] We contrast these CO distributions with that of atmospheric aerosols, which have shorter atmospheric lifetimes. Figure 4 shows the spatial distributions of multiyear seasonal average clear-sky AOD as observed by MODIS and CALIOP (daytime observations) and as predicted by GEOS-Chem. AOD is sampled in Figure 4 for coincident observations of MODIS and CALIOP to allow for direct comparison. In general, the observations and model give a consistent picture of the major source regions such as East China, the Eastern U.S. and the dust region in northern Africa with some differences in other regions such as the western U.S. (as previously noted by *Li et al.* [2005] and *van Donkelaar et al.* [2010]). The model also captures the seasonal evolution of export from the major Northern Hemisphere source regions observed by the two instruments. The greatest outflow from Asia is in the spring; although, compared to the other regions, there is substantial export in all seasons. Outflow from the eastern U.S. also occurs in all seasons, though based on the observations here, the pathways are different. In winter, aerosols are transported at higher latitudes than in spring and summer [*Stohl and Eckhardt*, 2004]. European emissions tend to remain more localized or be transported over other emission regions, making export generally more difficult to distinguish from local emissions.

[34] While there are noted issues with the simulated dust transport off western Africa in GEOS-Chem [*Generoso et al.*, 2008] and a high bias in the dust AOD due to the assumed sub-micron size distribution of dust in the model [*Ridley et al.*, 2012], here we focus on export out of industrial regions in the midlatitudes where the transport of aerosols has the greatest potential to impact downwind air quality (we do not investigate transport to the Arctic in this work). We note that dust from Africa contributes to AOD over Europe (and sometimes over the U.S.) in all seasons and can slightly bias simulated AOD values; however, this impact is most prominent in the spring season and does not dominate the total simulated AOD over Europe in GEOS-Chem.

[35] Figure 4 shows that MODIS observations are higher than CALIOP throughout the Northern Hemisphere. MODIS is generally higher than both CALIOP and GEOS-Chem over the oceans, in agreement with previous studies that suggested that MODIS might be biased high at low loadings [*Levy et al.*, 2005; *Remer et al.*, 2005; *Heald et al.*, 2006] and previous comparisons between MODIS and CALIOP discussed in section 3.3. The scatterplots in Figure 5 and

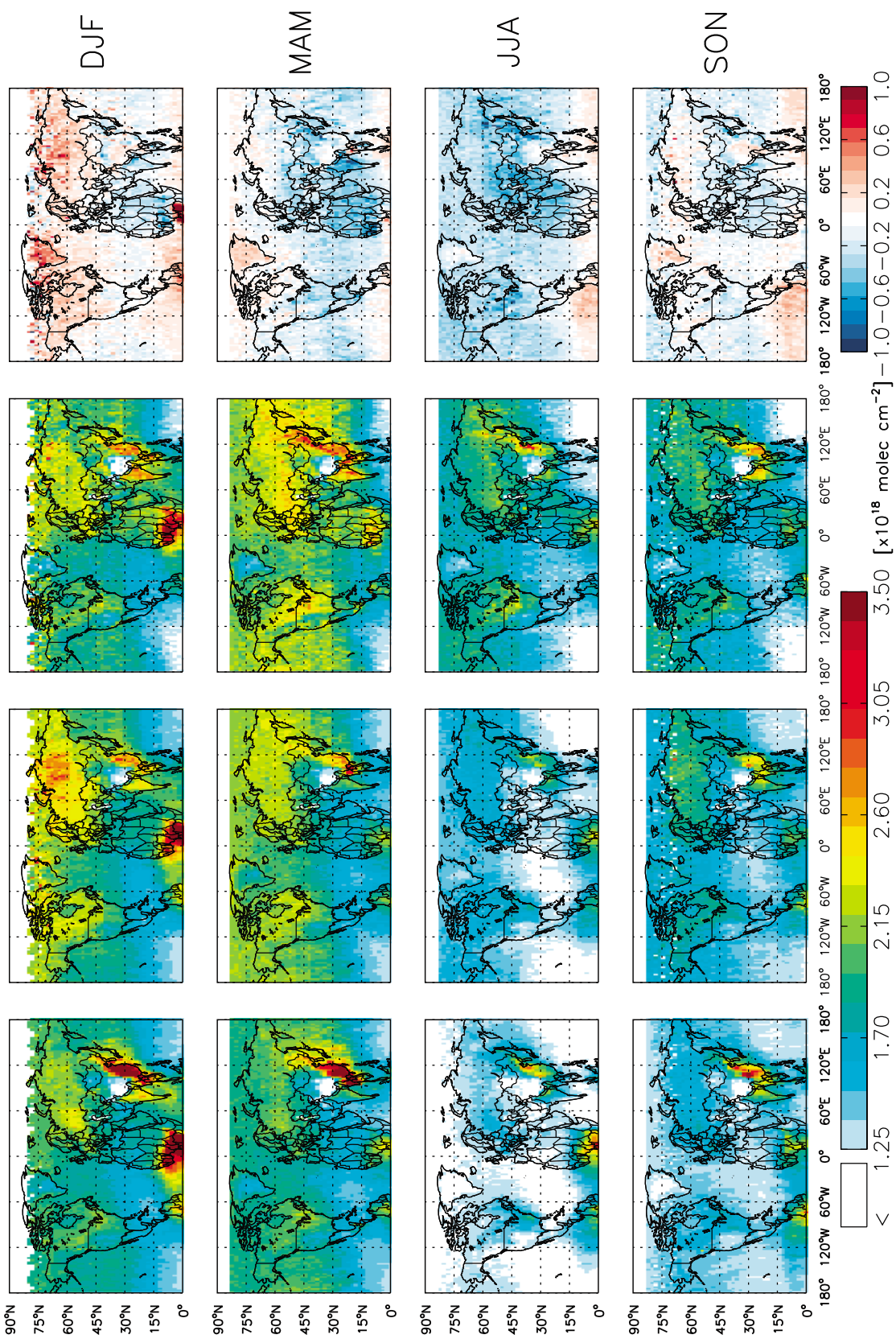

Figure 3. Seasonal mean CO atmospheric column concentrations for three years (December 2006–November 2009) from (left to right) GEOS-Chem sampled for TES overpass time and location and interpolated to TES vertical levels, GEOS-Chem with the TES operator retrieval applied, TES, and the difference (GEOS-Chem with retrieval operator applied minus TES). The GEOS-Chem simulation is sampled for TES overpass times and locations. Color bars are saturated at 3.5×10^{18} molecules/cm^2 and $\pm 1 \times 10^{18}$ molecules/cm^2 respectively.

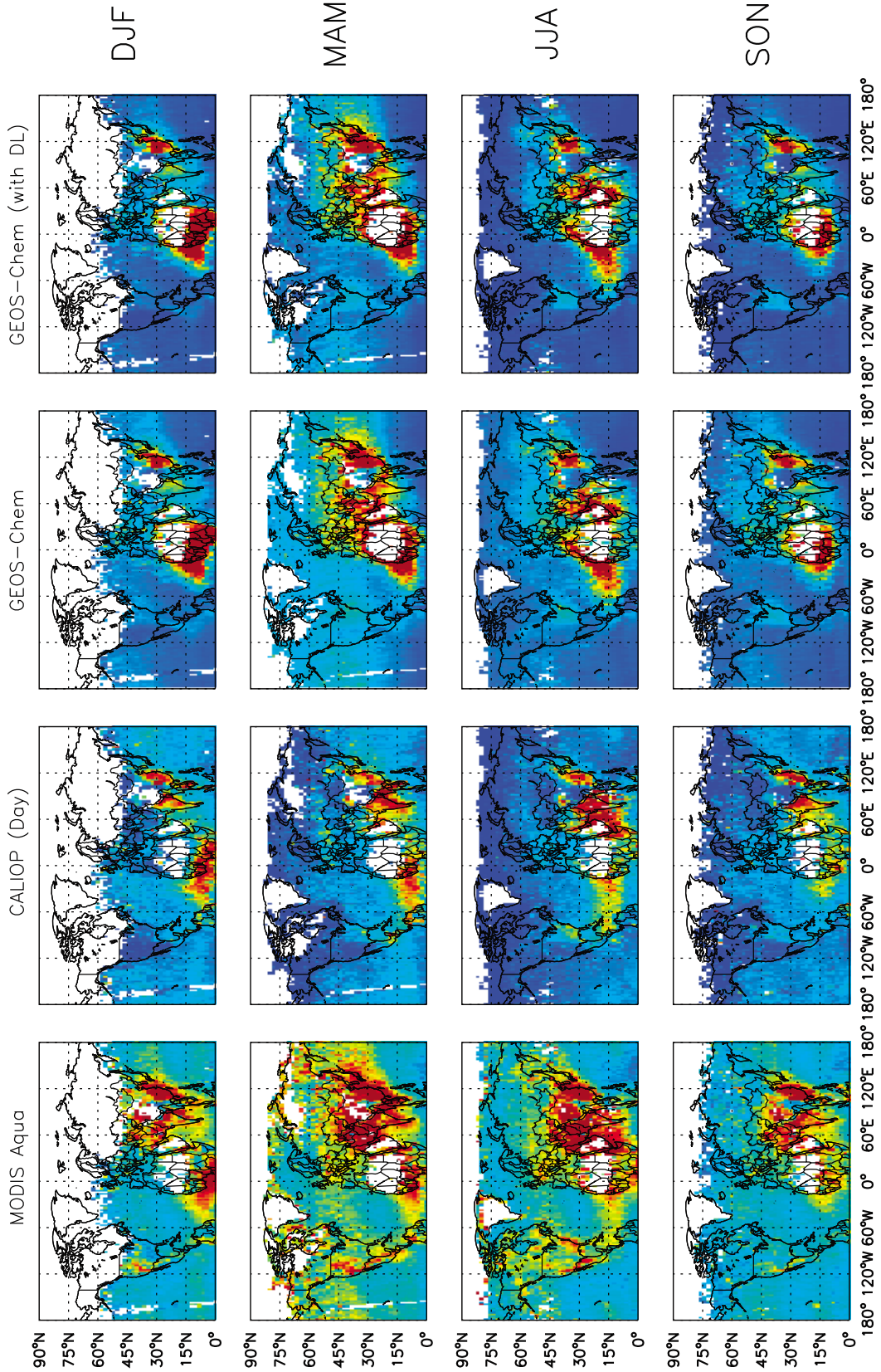

Figure 4. Seasonal means (organized by row) of aerosol optical depth as observed by MODIS Aqua (column 1), CALIOP (daytime observations (column 2)), and as simulated by GEOS-Chem unfiltered (column 3) and filtered as discussed in section 4.1 (column 4) for three years (December 2006–November 2009); all are sampled for valid MODIS and CALIOP observations. The color bar is saturated at 0.5.

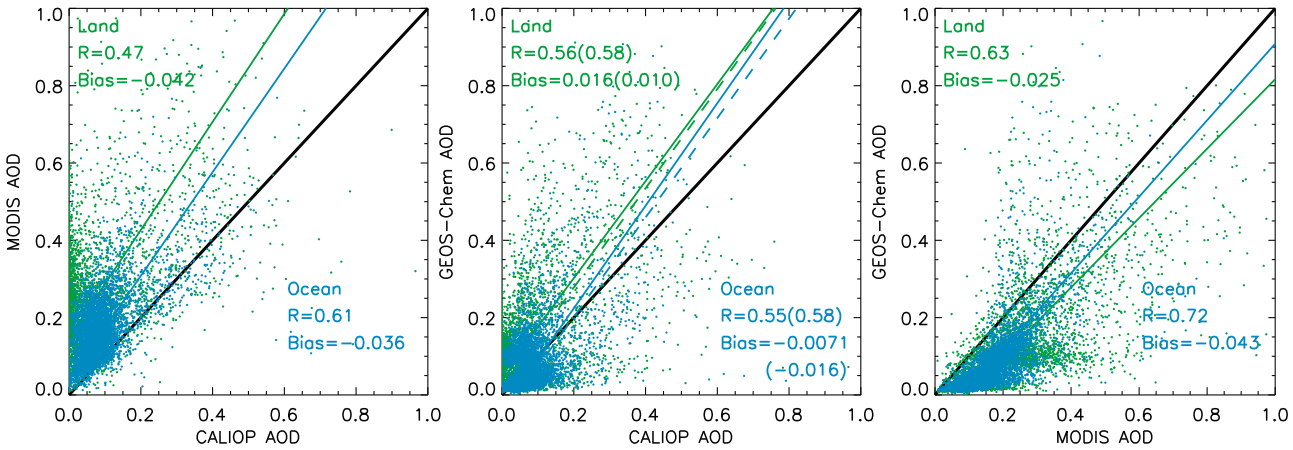

Figure 5. Scatterplots of three-year mean (2007–2009) springtime AOD from Figure 4 for MODIS and CALIOP, GEOS-Chem and CALIOP, and GEOS-Chem and MODIS. Ocean AOD statistics are in blue and land AOD statistics are in green. Correlation and average AOD bias are given in plot (for normalized mean bias, see Table 2). Values in parentheses are for GEOS-Chem simulated AOD with applied detection limit (see section 4.1).

statistics in Table 2 show that MODIS is generally higher than CALIOP both over ocean (mean AOD bias 0.042) and land (0.036) in the Northern Hemisphere (only spring is shown, but statement holds for all seasons), and especially over Asia as shown in Figure 4. Percentage normalized mean biases are given in Table 2. Part of the difference between the distributions observed by CALIOP and MODIS may be due to a misclassification of thick aerosol layers in the CALIOP algorithm [*Liu et al.*, 2009; *Yu et al.*, 2010] and only using cloud free profiles from CALIOP, which removes any profiles where aerosol and light cloud are mixed. Figure 5 also shows that the observation are better correlated over ocean (R = 0.61) than over land (R = 0.47), reflecting the challenges of characterizing surface reflectivity over land in aerosol retrievals.

[36] Comparing the spatial maps in Figure 4, we see that the simulated AOD (when no detection limits are applied) generally lies between the values reported by MODIS and CALIOP. For example over land the mean AOD bias in GEOS-Chem AOD is 0.016 for CALIOP and −0.025 for MODIS (Table 2). However, AOD is better correlated with MODIS (R = 0.72 over ocean and 0.63 over land) than CALIOP (R = 0.55 over ocean and R = 0.56 over land).

[37] Applying the CALIOP detection limits to the simulated aerosol profiles improves the correlation between GEOS-Chem and CALIOP, over the oceans (R = 0.55 to R = 0.56) and over land (R = 0.56 to R = 0.58). The model high bias over land is reduced (0.016 to 0.012), reflecting the inability of CALIOP to detect low aerosol extinction. However, while the spatial correlation is improved over marine regions, the bias increases (−0.0071 to −0.010 AOD). This is evident from the average AOD in Figure 4, which shows that introducing the detection limits to the GEOS-Chem simulated AOD primarily reduces values in remote marine areas, where there is already a low bias in comparison with CALIOP observations. Using a greater value for the detection limit further reduce the bias over land, but increases the bias over the ocean. While this filtering corrects for the inability of CALIOP to detect thin, dilute plumes, an important source of variability and aerosol loading over the clean oceans, this supports previous work that suggests that GEOS-Chem is under predicting marine aerosol [*Jaeglé et al.*, 2011; *Lapina et al.*, 2011]. We further investigate the impact of applying these detection limits by examining the distribution of aerosol species identified by the CALIOP algorithm and simulated with GEOS-Chem.

4.2. Distributions of Aerosol Species

[38] Figure 6 shows the average annual observed contribution to AOD from the six aerosol types classified by the CALIOP algorithm compared with the closest matching aerosol species simulated by GEOS-Chem with the detection limit applied. This is not a perfect match, as some CALIOP 'types' include several aerosol species. On average, dust and polluted dust make the strongest contribution to AOD in the Northern Hemisphere, and this contribution is heightened in spring months. The dust signal in GEOS-Chem is much stronger than the combined contribution from dust and polluted dust observed by CALIOP, attributable to biases in the sub-micron dust size distribution [*Ridley et al.*, 2012]. However, CALIOP also reports a strong polluted dust signature over India which is not captured by the model either as dust or inorganic (sulfate) aerosol. AOD from continental pollution is split between two CALIOP aerosol types (polluted

Table 2. Statistics for MODIS, CALIOP and GEOS-Chem Daytime AOD Comparisons for Spring Seasons (March, April, and May 2007–2009)[a]

	R		AOD Mean Bias		Normalized Mean Bias (%)	
Comparison	Land	Ocean	Land	Ocean	Land	Ocean
CALIOP-MODIS	0.47	0.61	−0.042	−0.036	−68%	−45%
GEOS-Chem-MODIS	0.63	0.72	−0.025	−0.043	−41%	−54%
GEOS-Chem-CALIOP	0.56	0.55	0.016	−0.0071	72%	−16%
Filtered G-Chem-CALIOP	0.58	0.58	0.010	−0.016	44%	−37%

[a]For the CALIOP and MODIS comparison, the normalized mean bias (NMB) is calculated by normalizing to MODIS. For all instrument and GEOS-Chem comparisons, the NMB is normalized to the instrument AOD.

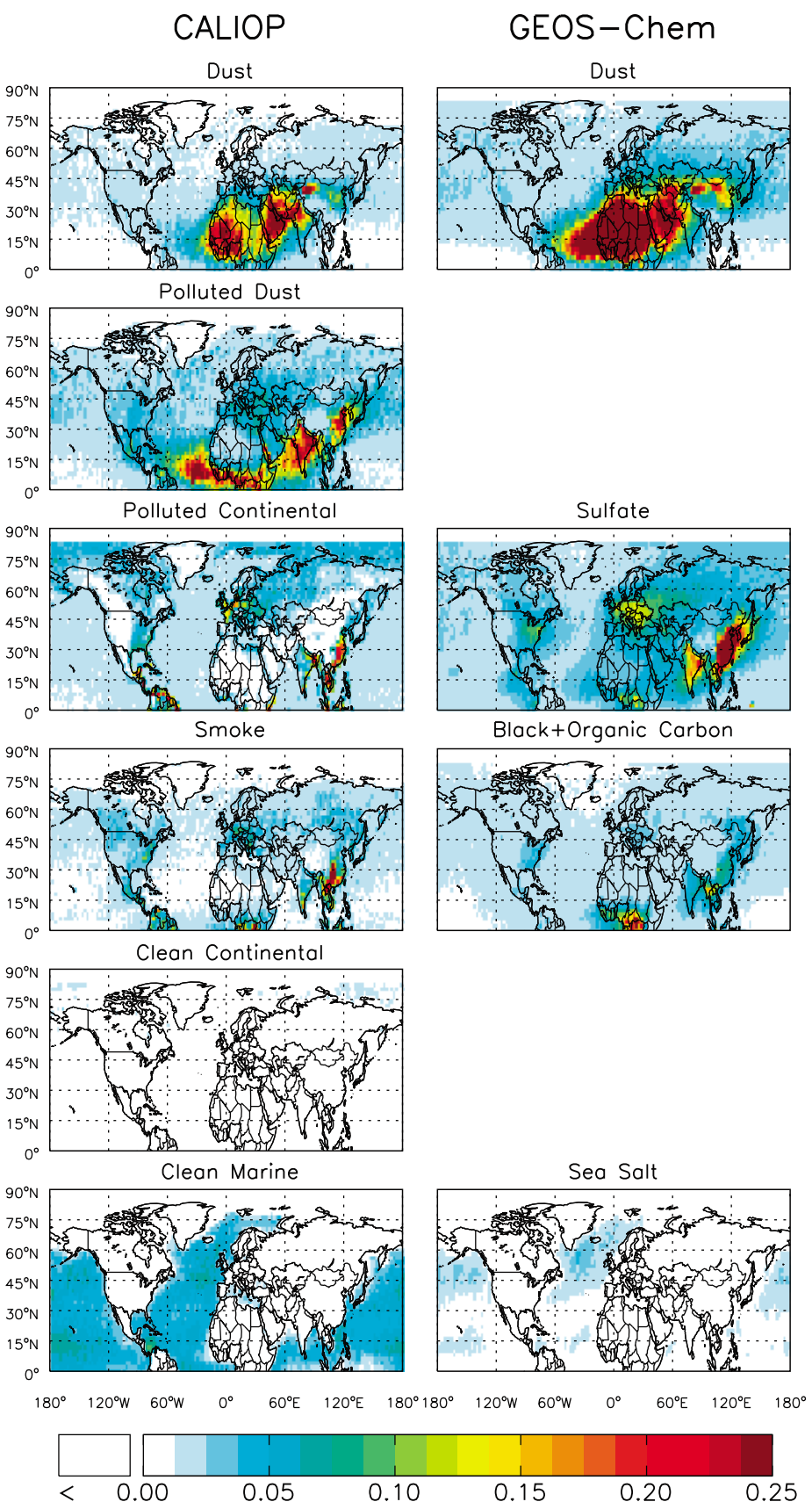

Figure 6. Average AOD contribution from each aerosol type from (left) CALIOP observations and (right) species as simulated by GEOS-Chem with the detection limit applied for 3 years (December 2006–November 2009). "Not determined" CALIOP subtype is not shown, because contribution is 0 everywhere.

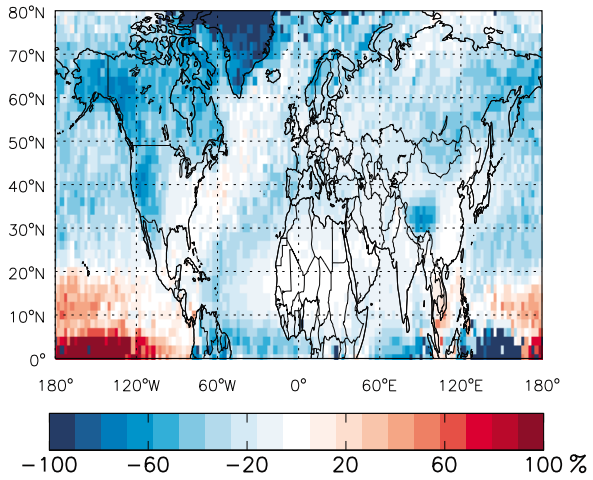

Figure 7. Percent difference between GEOS-Chem average total AOD (December 2006–November 2009) with only detection limits applied to species and GEOS-Chem average total AOD when only one species is "retrieved" at each pressure level.

continental and polluted dust). The distribution and magnitudes of these taken together, are consistent with simulated AOD from inorganic aerosol in GEOS-Chem (although not all inorganic aerosols are from pollution sources).

[39] GEOS-Chem does not simulate the strong BC/OC sources over Southeast Asia that stand out in the CALIOP observations of smoke aerosol. Additionally, over many other source regions of smoke (Russia, western Canada, South America), CALIOP smoke AOD is greater than GEOS-Chem simulated BC/OC AOD. Since CALIOP chooses a single dominant aerosol type and smoke aerosol has the highest lidar ratio, it is expected that the CALIOP AOD would be greater than as simulated by GEOS-Chem near smoke sources. However, GEOS-Chem simulates slightly higher AOD due to BC/OC transported over the oceanic regions than what CALIOP determines to be smoke aerosol (although both show that the contribution to total AOD is small). While there are sources of BC/OC not associated with smoke, part of this discrepancy is also due to the fact that the CALIOP classification algorithm (used when the lidar ratio cannot be calculated directly using the transmittance method [*Omar et al.*, 2009]) only allows for smoke aerosols to be classified in elevated layers [*Omar et al.*, 2009]. In GEOS-Chem, an average of 10–30% of carbonaceous AOD occurs in the boundary layer (up to 99% near sources), where it would not be identified by the CALIOP algorithm as smoke. Similarly, all elevated non-dust aerosol layers over the ocean are classified as smoke and cannot be classified as clean marine or polluted continental in the retrieval. Clean continental aerosols make their largest contribution to AOD over land and Arctic regions. Although this subtype was determined using measurements from a backscatter nephelometer [*Vaughan et al.*, 2004]; it is unclear what speciation or source of these aerosols is being represented. However, the contribution to AOD is very small (maximum of 0.03) and makes little impact on our comparisons here.

[40] CALIOP observes long range transport of dust, polluted dust, polluted continental aerosols and smoke aerosols over ocean basins. However, the contribution from each of these individual sources is generally smaller than the contribution from clean marine aerosols. The exception is for polluted dust and dust off western Africa and eastern China. GEOS-Chem sea salt AOD is also lower than the clean marine aerosols from CALIOP (as in Figure 6), which is partly due to a bias in sea salt distribution in GEOS-Chem [*Jaeglé et al.*, 2011] and the fact that the aerosol type "clean marine" likely also includes organic and sulfate aerosols of oceanic origin.

[41] Comparing these distributions of aerosol species types with the total AOD comparisons in Figure 4 suggest that the overall high bias of GEOS-Chem compared to CALIOP continental AOD (Figure 5) is mostly due to African dust over the Middle East and Europe and pollution over Asia. The overestimation of dust is possibly masking other issues that would impact the total column AOD in outflow regions (Figure 4), such as the underestimate in marine regions and export of polluted and smoke aerosols from Europe.

[42] We also examine the effect several constraints of the CALIOP retrieval algorithm might have on total AOD. CALIOP classifies each observed layer as only one aerosol subtype, and therefore uses only one lidar ratio for that observed layer, whereas the model may include contributions from several aerosol species in a given layer. In order to examine the effect this would have on total AOD, we "retrieve" only one aerosol species for each GEOS-Chem pressure level as well. To do this, we determine the dominant aerosol type, and multiply all other aerosol type extinction values by a ratio of the dominant aerosol lidar ratio to the lidar ratios of the other aerosol types present (lidar ratios listed in Table 1). For a single layer, the change is linear. However, for the total AOD, the result is more complex, with values affected not only by the different lidar ratio, but also how the type impacts the extinction detection limits applied. Figure 7 shows the resulting percent difference in total simulated AOD. In general, this leads to a 10–30% decrease in total AOD in the midlatitudes, with even larger percent changes in regions with low aerosol loading. In marine atmospheres, this is because sea salt aerosols dominate and have the lowest lidar ratio. In many other regions this is due to dust being the "dominant" aerosol aloft (extinction values are very low), which also has a lower lidar ratio than pollution. Replacing simulated aerosol with these lower lidar ratios, reduces the total AOD, bringing the model into better agreement with CALIOP over the oceans. We conclude that assuming one aerosol type for each layer with a predetermined lidar ratio can bias the column AOD, but is part of a larger, complex issue of accurate selection of a lidar ratio for mixed aerosol.

5. Vertical Distributions of Pollutants

5.1. Hemispheric Cross-Sections and Comparisons With Observations

[43] While seasonality in emissions and pollutant lifetimes can account for many of the differences between the downwind impacts of CO and aerosols, there are also different export mechanisms that are not evident from the total column

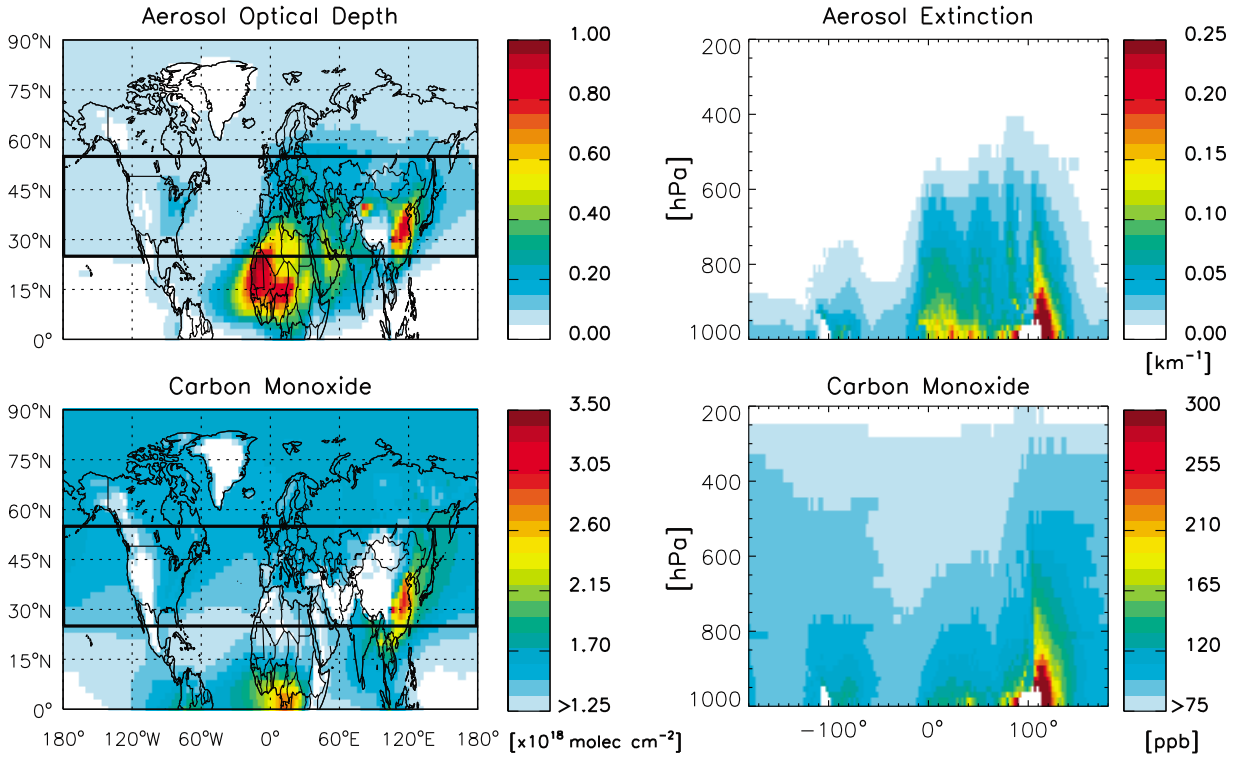

Figure 8. Annual average AOD and column total CO simulated by GEOS-Chem for three years (December 2006–November 2009). Box indicates region of averaging for vertical distributions of aerosol extinction and CO in the plots on the right. Note color bar scales.

spatial distributions. We therefore investigate the vertical distribution of LRT here.

[44] In order to investigate LRT on a hemispheric scale, we average the vertical distributions over a consistent latitudinal circle from 25°–55°N for all regions, as these are the latitudes at which transport most often occurs in the Northern Hemisphere. Expanding this range dilutes the export from some regions. However, as evident in Figure 8, this range does not include all of the British Isles, Canada, the Arctic, or all of Southeast Asia, but does include Northern Africa. We are therefore, missing some of the dominant transport pathways of European emissions, while including export from northern Africa which features stronger lofting than often noted for Europe.

[45] Figure 8 shows differences in the annual multiyear average distributions of CO and aerosols as simulated by GEOS-Chem. There is generally good spatial agreement in AOD and CO column totals near source regions, except in regions where dust is the primary contributor to aerosol concentrations. The shorter lifetimes of aerosols, however, is highlighted here by the strong gradients near the source, both vertically and horizontally, as compared to CO. In the region shown, CO in the middle troposphere (∼700 to 450 hPa) is on average 22% lower than in the lower troposphere (∼1000 to 800 hPa), while aerosol extinction is on average 75% lower. Even from these multiyear averages, we see that there is more lofting of CO compared to aerosols, which allows CO to be transported more efficiently downwind. As noted by *Heald et al.* [2006], CO from Asia is transported at all altitudes, while aerosols are generally transported distinctly in the lower free troposphere. This is a result of aerosols being scavenged more efficiently than CO during convective lifting and faster removal of aerosols in boundary layer outflow [*Heald et al.*, 2006].

[46] We compare the multiyear annually averaged vertical distributions of CO as measured by TES and as simulated by GEOS-Chem (with the TES retrieval operator) in Figure 9 (annual average only shown- seasonal maps are consistent with these results). As discussed previously, GEOS-Chem has an overall low bias compared to TES, shown here throughout the troposphere. This is especially evident over Europe where the difference is strongest during the spring and summer, as also seen by *Kopacz et al.* [2010] who suggested that European emissions were underestimated in GEOS-Chem. However, the coarse vertical resolution of the IR retrieval makes it difficult to evaluate the vertical distribution of the simulated CO and isolate biases in emissions from biases in lifetime. Because CALIOP has much finer vertical resolution than TES, examining the vertical distribution of aerosol extinction provides more insight into export of pollution out of each region. Therefore, in the following sections, we focus primarily on aerosol transport.

[47] Figure 10 shows the seasonal averages of the vertical distribution of aerosol extinction as measured by CALIOP, simulated with GEOS-Chem (initially without detection limits applied) and the differences between the two (3rd column). We then show a more accurate comparison of the two when the CALIOP detection limits are applied to GEOS-Chem

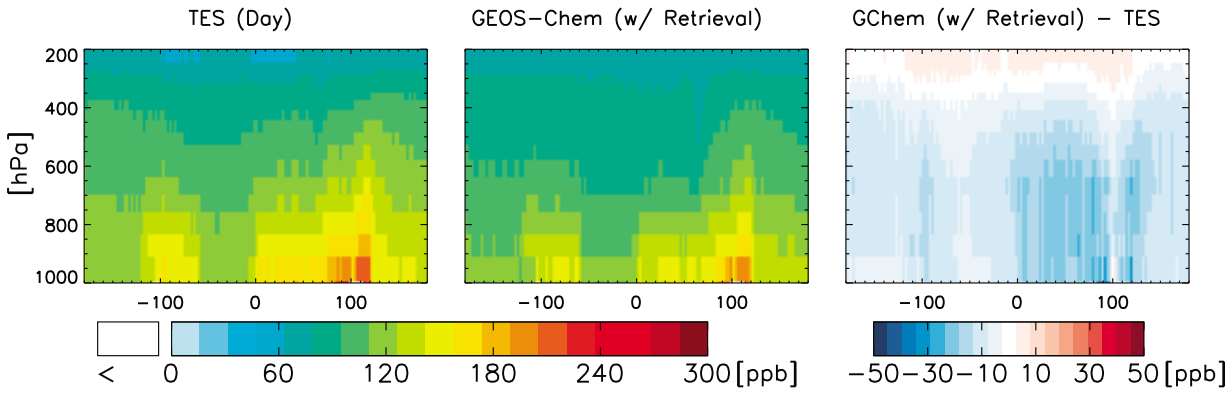

Figure 9. Annual average of the vertical distribution of CO averaged from 25 to 55°N for December 2006–November 2009 from TES and GEOS-Chem with the TES retrieval operator, and the difference. GEOS-Chem is sampled to match TES overpass time and location. The color bars are saturated at respective maximum values.

(4th column, as discussed in section 3.2). Both comparisons are shown to illustrate the importance of accounting for detection limits, particularly aloft, where doing so reduces the model-measured bias. This reflects the inability of CALIOP to detect dilute plumes, which may hinder the ability of CALIOP to track aerosol long range transport and characterize the contribution that this makes to the hemisphere aerosol background. However, even with detection limits applied it is clear that GEOS-Chem overestimates aerosol extinction aloft throughout the Northern Hemisphere. As shown previously, GEOS-Chem reproduces the strong source signatures observed by CALIOP, although it is often biased high in these source regions, including over Asia (at ∼90°–120°E) and over Europe/Northern Africa (∼0°) compared to CALIOP. Figure 4 shows that CALIOP is lower than GEOS-Chem and MODIS over land, suggesting that there could be an issue with the CALIOP retrieval (sections 2.1 and 3) and not necessarily a model error. However, aerosol extinction aloft and downwind of Asia, where misclassification is less likely to contribute, is also biased slightly high, suggesting that either Asian emissions or vertical lofting in the model are somewhat overestimated.

[48] Aerosol extinction over North America in spring and summer is underestimated in GEOS-Chem. Both CALIOP and MODIS show strong enhancements over the southeastern U.S. that are not simulated by GEOS-Chem, indicating that the discrepancy in the vertical distributions is most likely due to a missing source, possibly biogenic in nature, as suggested by *Goldstein et al.* [2009].

[49] Simulated aerosol extinction is consistently lower than observed by CALIOP at the low altitudes over ocean basins. This suggests that either CALIOP observations support more efficient export of pollution via boundary layer outflow and advection with the mean wind or that GEOS-Chem could be missing some more important background sources in marine regions. *Lapina et al.* [2011] show that this model underestimate of AOD occurs throughout the remote oceans, and therefore is not likely limited to pollution export biases. Figures 10 and 4 demonstrate that compensating biases, in outflow aloft and near the surface, can be masked in total AOD comparisons and that an accurate examination of long range transport requires information on the vertical distribution of pollutants.

5.2. Cross-Sections of Aerosol Species Extinction

[50] The contribution of each aerosol type determined by the CALIOP algorithm to the total aerosol extinction is shown in Figure 11 (left). The main aerosol type in the boundary layer is clean marine over the ocean basins and polluted (dust and continental are combined in Figure 11) over land. At higher altitudes, dust dominates over Northern Africa/Middle East, while polluted dominates elsewhere. Smoke aerosols also make a modest contribution to aerosol extinction aloft.

[51] Figure 11 also compares the aerosol extinction from CALIOP with the values simulated for GEOS-Chem species (with detection limits applied). This identifies excess dust over North Africa as the cause of the model overestimate over Europe/North Africa, as seen in Figure 10, while the discrepancies over Asia and North America are due to pollution species.

[52] GEOS-Chem distributions of BC/OC capture the magnitude of smoke extinction reported by CALIOP aloft. Most of the discrepancies from the AOD maps (Figure 4) are due to differences near the surface and the aforementioned facts that there are other sources of BC/OC and that the CALIOP algorithm only identifies smoke aerosols in elevated layers [*Omar et al.*, 2009]. At low altitudes, CALIOP generally identifies these aerosol layers as polluted continental, which has the same lidar ratio as smoke (Table 1), and therefore a miscategorized layer would not impact the total extinction (or AOD). However, it does complicate the comparison here between GEOS-Chem inorganic species and CALIOP polluted aerosols because CALIOP will not categorize lofted layers as polluted continental (except over snow/ice/tundra).

[53] Figure 11 shows that the majority of the aerosol that CALIOP observes in low level outflow is clean marine, with some contribution from polluted aerosols. Comparing the polluted aerosols and the simulated inorganic (sulfate) aerosol extinction does suggest that GEOS-Chem has a slight underestimate in low level pollution transport. However,

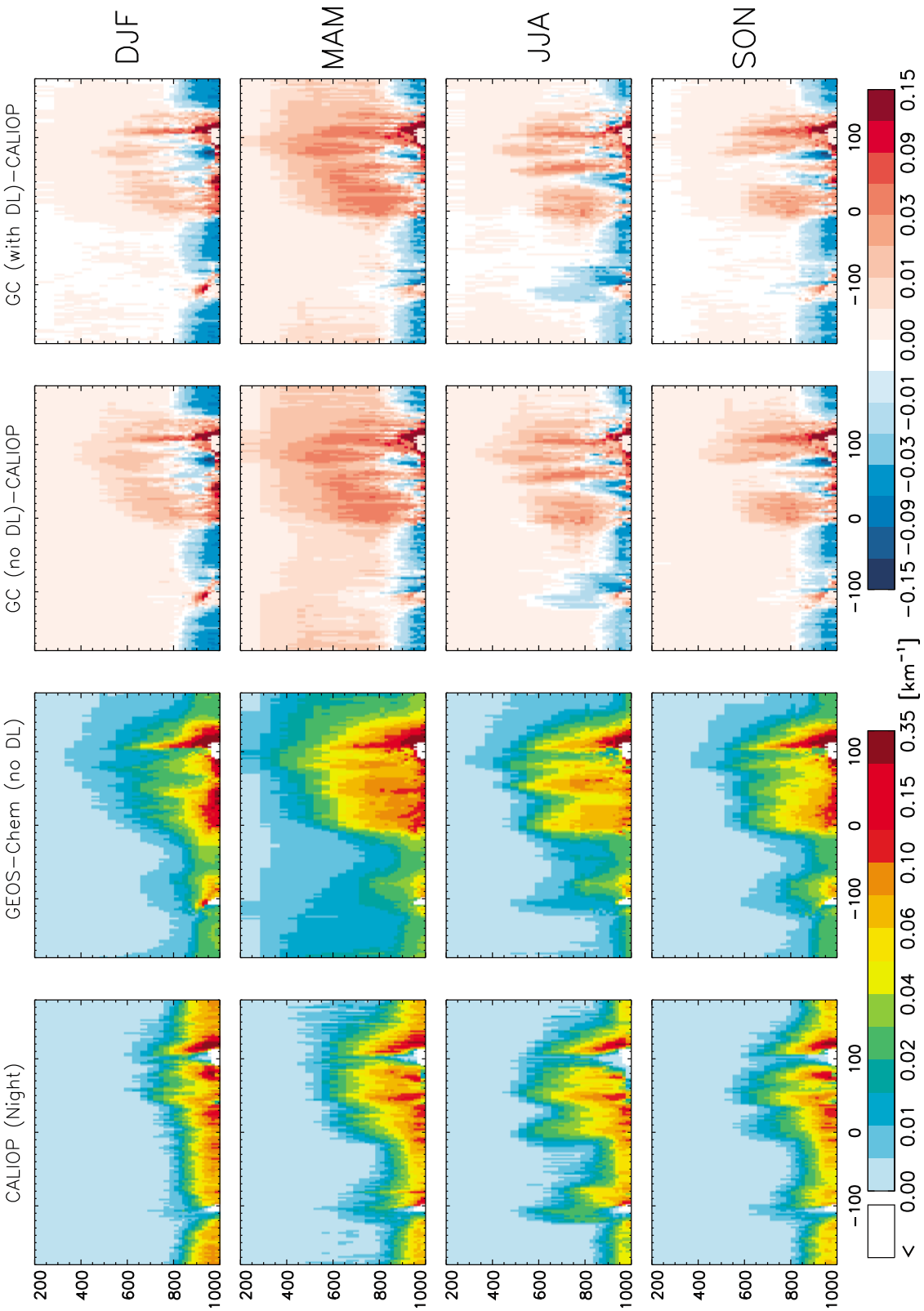

Figure 10. Seasonal averages of aerosol extinction averaged from 25 to 55°N as observed by CALIOP (night observations only (column 1)) and simulated by GEOS-Chem (column 2). Column 3 is the difference (GEOS-Chem – CALIOP) for GEOS-Chem output and column 4 is the difference when CALIOP detection limits are applied to GEOS-Chem values. GEOS-Chem is sampled to match CALIOP overpass time and location. The color bars are saturated at respective maximum values.

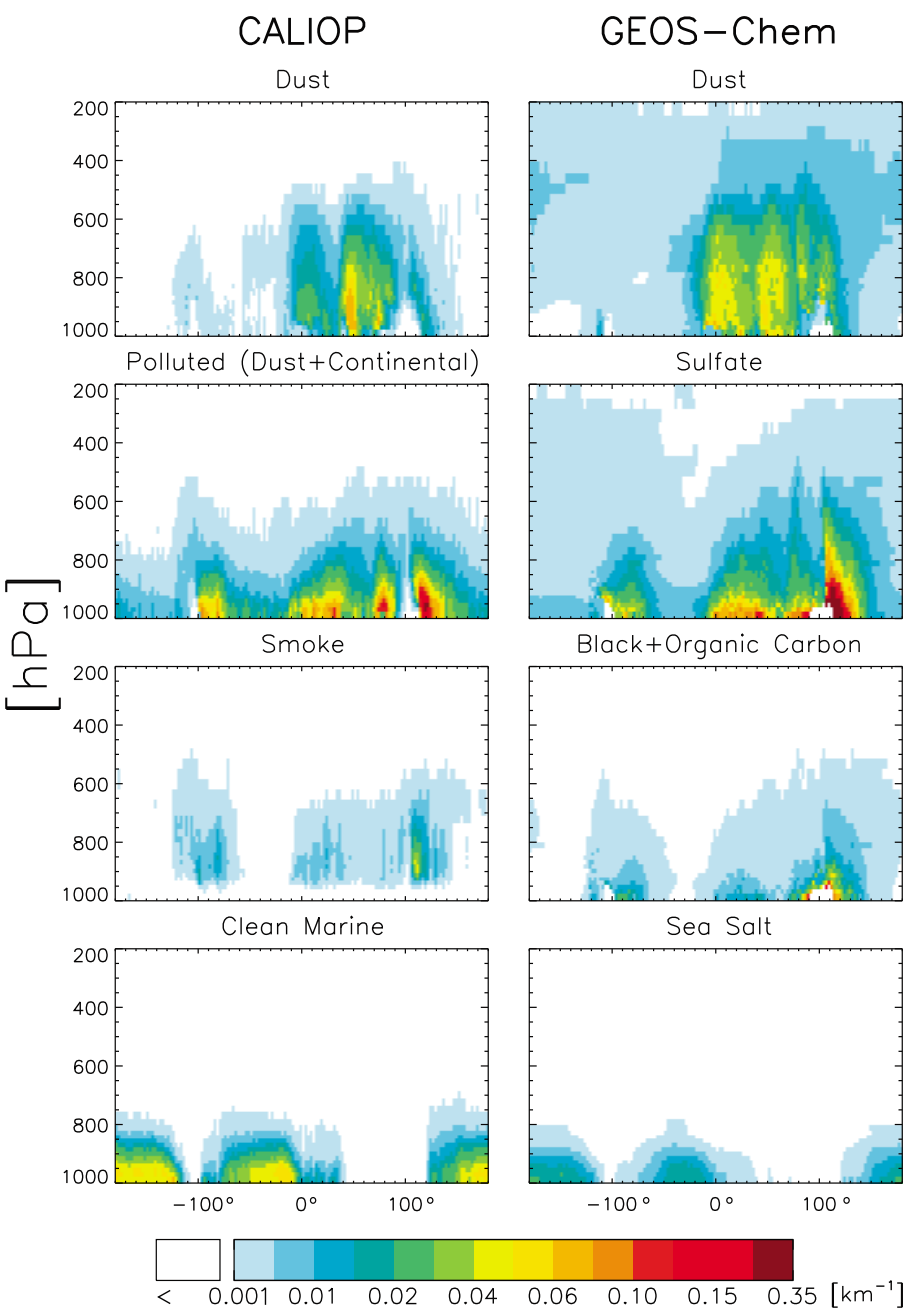

Figure 11. Average extinction contribution from species type (left) from CALIOP observations and (right) as simulated by GEOS-Chem, with CALIOP detection limits applied for December 2006–November 2009, averaged from 25 to 55°N. CALIOP "Not determined" and "clean continental" subtypes are not shown, because contribution is 0 and < 0.005 everywhere. Note color bar scale.

Figure 6 shows that the underestimate in GEOS-Chem sea salt compared to CALIOP clean marine aerosols extends beyond outflow regions to more remote marine regions, suggesting that the main discrepancy in marine atmospheres is due to a missing source of marine aerosol and only partially due to an underestimate of pollution aerosol in outflow regions.

[54] GEOS-Chem simulates excessive dust and sulfate transport aloft compared to CALIOP observations even with the detection limits applied. These are very small values of less than 0.005 km^{-1} when averaged over the latitudinal bands. These are most likely still below the actual detection limit of CALIOP which is altitude-dependent and is only roughly 2–4 × 10^{-4} km^{-1} sr^{-1} [*Winker et al.*, 2009].

[55] These comparisons assume that the CALIOP algorithm is correctly attributing aerosol types (and using the correct lidar ratio). Clean marine aerosols have the lowest lidar ratio (which *Oo and Holz* [2011] and *Sayer et al.* [2012] claim is often too low) in the CALIOP algorithm (Table 1), therefore, if CALIOP incorrectly identifies polluted or smoke aerosols as clean marine, then the aerosol extinction (and optical depth) determined by CALIOP could be biased low

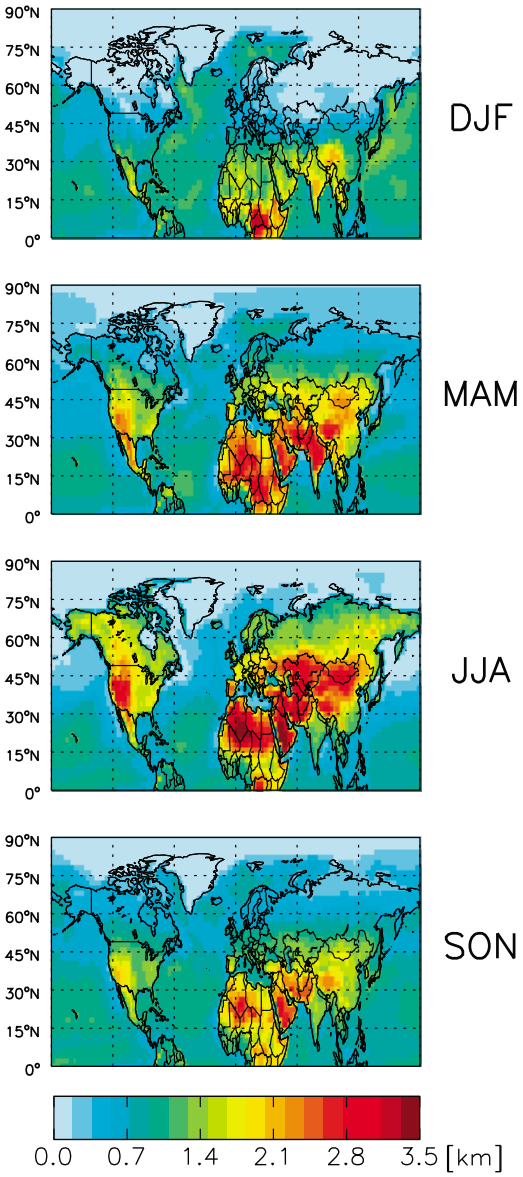

Figure 12. Seasonal averages of daytime planetary boundary layer heights from GEOS5 sampled to coincide with A-train crossover time. The color bar is saturated at maximum value.

[*Yu et al.*, 2010], and the total extinction difference could be even greater than determined in Figure 10.

6. Fraction of Pollutants in the PBL

[56] *Deeter et al.* [2007] have shown that the vertical information in CO retrievals generally comes from two regions: the lower troposphere and the middle troposphere. We attempt to exploit the constraints offered by TES on the vertical distribution of CO by examining the fraction of the CO column in these two regions.

[57] To differentiate the lower troposphere, we use daily output PBL heights from GEOS-Chem coincident with the satellite overpass. We chose to use specific PBL heights rather than a cutoff pressure level in order to better reflect atmospheric distributions and transport mechanisms. PBL heights can also have a strong impact on the vertical distribution of pollutants and vary with season and location [*Lin and McElroy*, 2010]. Figure 12 shows the seasonal averages of PBL heights from GEOS-5 meteorology used here. Additionally, PBL heights have a strong diurnal cycle, varying by a factor of ~10 from day to night [*Lin et al.*, 2008]; for this reason, and the fact that emissions are normally greater during the day [*Lin and McElroy*, 2010], the following comparisons are made with daytime observations.

[58] A validation of the GEOS-5 PBL heights using CALIOP is presented by *Jordan et al.* [2010] and shows that GEOS-5 generally predicts PBL heights within 25% of CALIOP observations with regional and seasonal differences. Correlation coefficients are 0.47–0.73 in the Western Hemisphere and Africa, with lower values in December and higher values in August. As more thoroughly discussed by *Lin and McElroy* [2010], vertical mixing in the PBL can strongly influence the vertical distributions of gas and aerosol species. Therefore, in regions or seasons where GEOS-5 incorrectly represents the depth of the PBL, the fractions of CO or aerosols in the PBL that we present here might be under- or overestimated, but will require more extensive validation of PBL depths that is beyond the goal of this work. Seasonal averages of the fraction of the total column CO that is in the PBL as observed by TES and simulated by GEOS-Chem are shown in Figure 13. There are some regions where the lowest altitude with a valid observations from TES is above the PBL (over Himalayas and Greenland), fractions therefore cannot be calculated and are disregarded in our seasonal averages (white in Figure 13). We include the fraction of CO in the PBL simulated by GEOS-Chem both before and after applying the retrieval operator in order to substantiate that smoothing by the averaging kernels does not significantly change the results. Overall, TES and GEOS-Chem are in good agreement, although GEOS-Chem shows slightly less CO in the PBL in winter and fall, slightly higher fractions in summer, and a mix in spring. However, the difference is generally less than 5%.

[59] Figure 13 also shows the interaction of several factors that determine the amount of CO that remains in the boundary layer: emissions, boundary layer height, lofting mechanisms, and the lifetime of CO. Source signatures are often diluted with seasonal variability in PBL depths and oxidant loading. For example, Asia and India are important sources of CO throughout the year, but the fraction in the PBL is greatest in spring, when the PBL is highest. Elevated emissions and the suppression of convection in wintertime, lead to accumulation of CO in the PBL in winter/spring over this region. Fall generally has the least CO in the PBL throughout the Northern Hemisphere, which is in large part due to the significantly shallower PBL in GEOS-Chem, but also due to removal throughout the summer and decreases in emissions. Overall, given limitations in the vertical resolution of the observations, these comparisons do not reveal any definitive bias in the simulated vertical profile of CO, but may suggest that CO lifetime is too long in summer and too short in winter.

[60] We contrast these results with fractions of AOD in the PBL observed by CALIOP and simulated with GEOS-Chem in Figure 14. Again, we see the importance of accounting for the CALIOP detection limits in these comparisons, where not

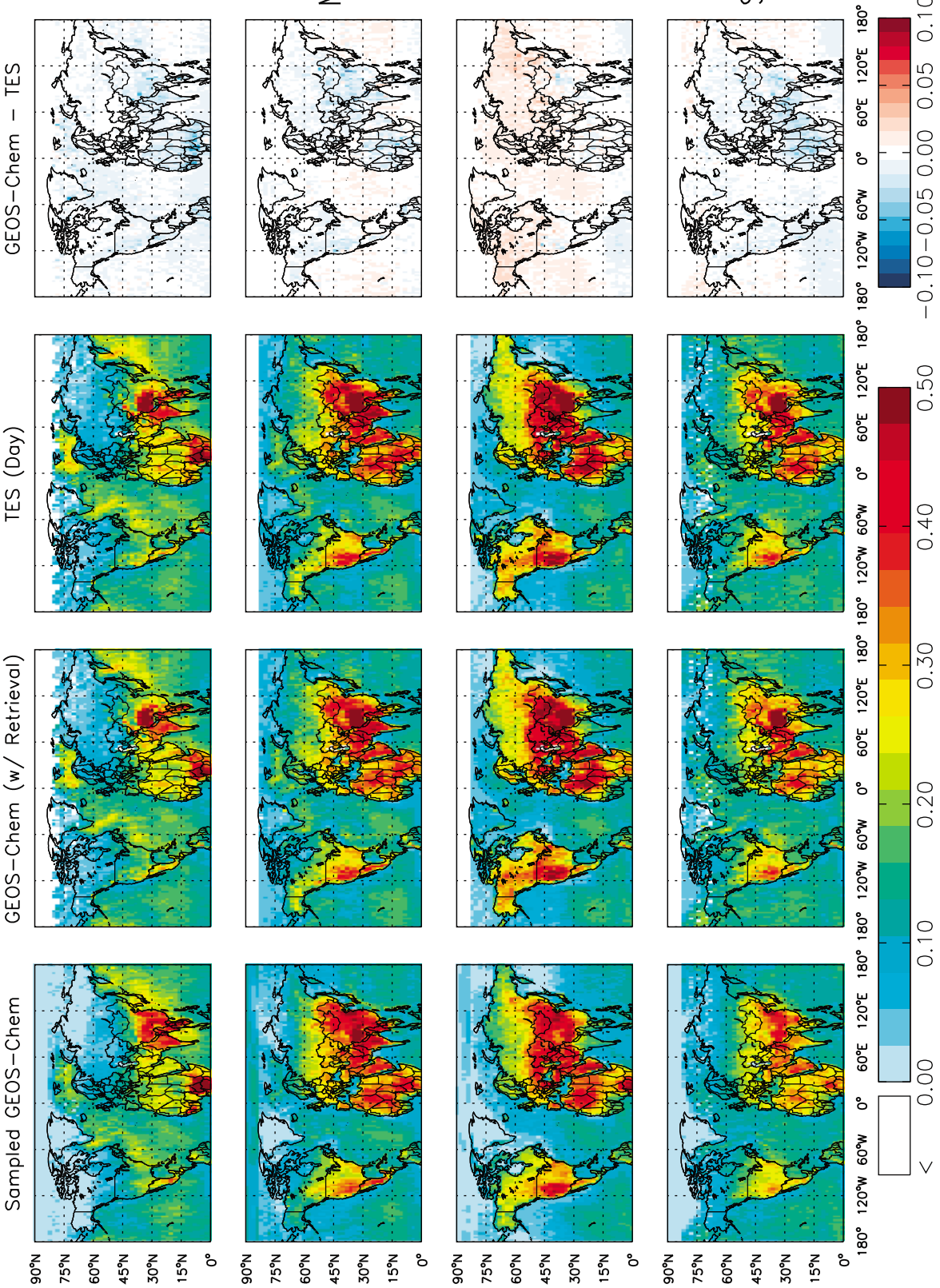

Figure 13. Seasonal distributions of the fraction of CO that remains in the PBL as simulated by GEOS-Chem (sampled to TES location), GEOS-Chem (with the TES retrieval operator), as observed by TES and the difference. The color bars are saturated at respective maximum values.

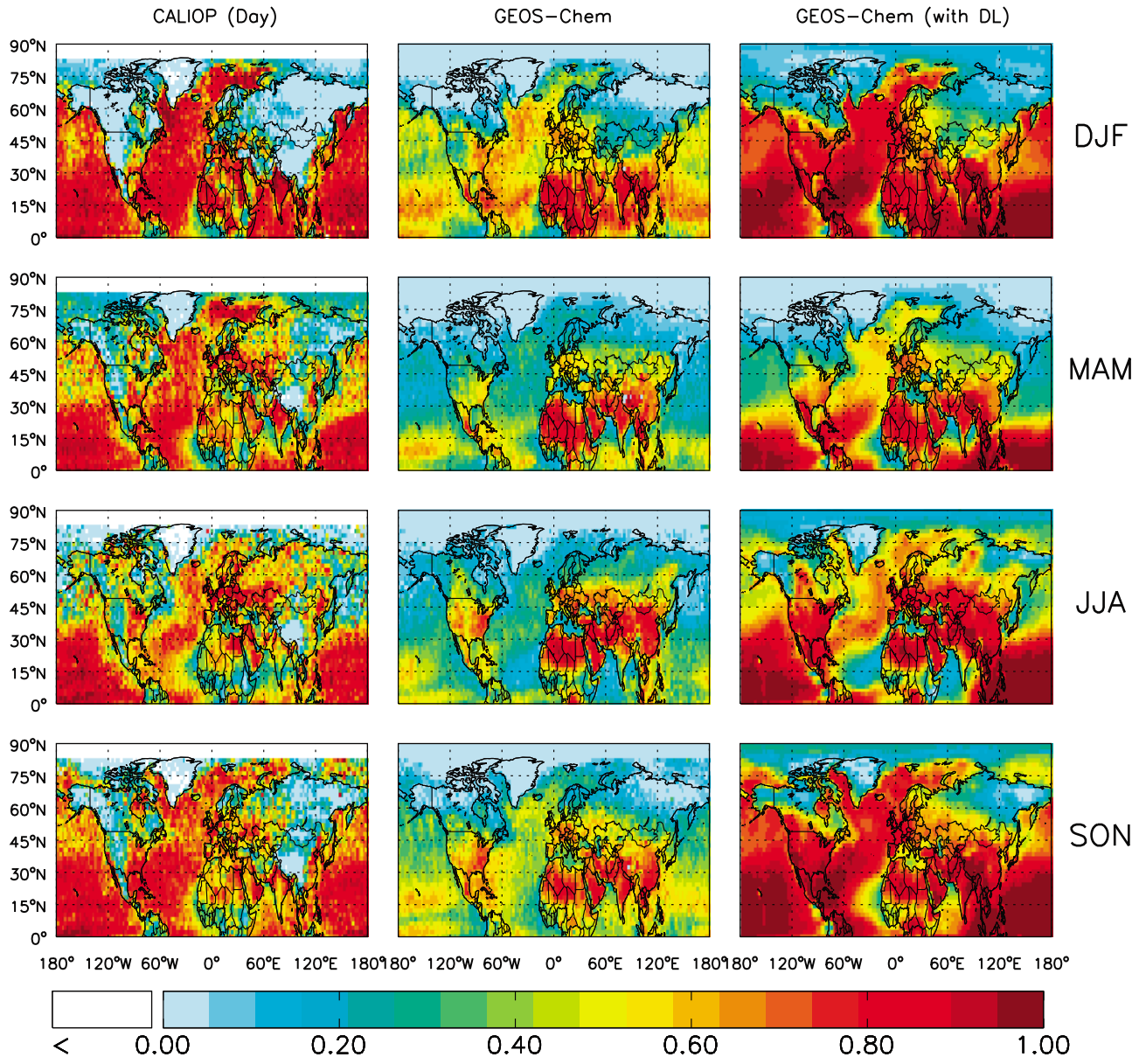

Figure 14. Seasonal distributions of the fraction of AOD that remains in the PBL (left) as observed by CALIOP and (middle) simulated by GEOS-Chem without the detection limit applied and (right) with the detection limit applied.

doing so substantially underestimates the fraction of aerosol extinction that be attributed to boundary layer aerosol.

[61] Both CALIOP and GEOS-Chem show higher fractions of aerosol in the PBL over source regions such as the eastern U.S., Europe and eastern China in spring and summer but those values drop in outflow regions (e.g., off the east coast of the U.S. and off Asia), indicating the vertical venting of exported pollution and the preferential removal of pollutants in the boundary layer. This is especially noticeable in spring and summer. The fraction of aerosol in the PBL off Asia is also generally lower than off the northeastern U.S., indicating more vertical lofting. This export difference is reproduced in the model. However, the PBL fractions in outflow over the oceans are noticeably different between CALIOP and GEOS-Chem. While a good portion of this is due to the aforementioned issues with instrument sensitivity and choice of detection limit; applying any detection limit to the model output still leaves inconsistencies in the spatial patterns, especially during spring and summer, seasons of the greatest amount of outflow. The gradient in the fraction of pollutants in the PBL from the source to outflow regions in GEOS-Chem is much more noticeable than with the CALIOP observations, indicating either (1) an excess of lofted aerosols near source in the model (e.g., over Asia), (2) too much removal of aerosols in the boundary layer, or (3) a missing source of aerosol in the boundary layer, or a combination thereof. In Figure 10, GEOS-Chem does have a stronger source signature over Asia that leads to a greater amount of aerosols aloft, while also simulating much lower extinction in the boundary layer outflow region.

[62] The model also significantly overestimates the fraction of aerosols observed in the PBL over Asia and the western United States, year-round. From Figure 10, this overestimation over Asia appears to be due to a model overestimate of the source signature at the surface, which again may be attributed to misclassification of aerosols as clouds in the CALIOP retrieval. Over the western United States, it is a combination of slightly more predicted aerosol near the surface, and missing aerosol aloft.

[63] The seasonality in fractional PBL aerosol loading peaks in the winter, unlike CO, reflecting primarily the shallower winter PBL and suppressed vertical mixing. Near sources, ~80% of the aerosols are in the boundary layer, but for CO these values are rarely over 50%, again emphasizing the much larger background concentrations of CO that reside in the free troposphere.

7. Conclusions

[64] We use observations from three A-train satellites: CALIOP, MODIS, and TES in conjunction with a global chemical transport model (GEOS-Chem) in order to analyze the vertical features of CO and aerosol in the Northern Hemisphere. To make accurate comparisons, we sample the model output to the satellite overpasses; in doing so, we find that the limited spatial coverage of the CALIOP and TES instruments inhibited our ability to track specific plumes. However, we find that on seasonal time scales this sampling of the model produced little bias. Therefore, rather than analyze individual episodic transport events as many previous studies have done, we use observations from three years (December 2006–November 2009) and conduct three year-long simulations with GEOS-Chem in order to compute multiyear seasonal averages of vertical distributions.

[65] We find that the GEOS-Chem simulation is biased low in comparison to TES CO and MODIS AOD, but biased high in comparison to CALIOP AOD over land and aloft. Some of the discrepancies between MODIS and CALIOP AOD are in regions of heavy outflow (dust from western Africa and pollution off Asia) and most likely due to a miscategorization of thick aerosol layers as clouds by the CALIOP algorithm or the removal of these thick layers during our filtering process. Using a stricter cloud fraction cutoff for MODIS could potentially improve the comparisons with CALIOP. Applying a detection limit to the simulated AOD values is also necessary for making a more accurate comparison to CALIOP observations.

[66] We use a simple method for applying a detection limit to the GEOS-Chem simulation where we use the aerosol type lidar ratios from CALIOP to convert extinction profiles to backscatter values and assume that the detection limit is 2×10^{-4} km^{-1} sr^{-1} throughout the atmospheric column. We do not take into account differences in the detection limit at differing altitudes, nor did we systematically attempt to retrieve a single species for each pressure level as in the CALIOP algorithm. We do show that mimicking a retrieval of a single species in GEOS-Chem output can decrease total AOD by 10–30% at midlatitudes. This highlights the key issue of assessing lidar ratios accurately and the challenge in comparing with models that simulate mixed aerosol types. Even the application of a single, low detection limit improves our comparisons, especially aloft, reflecting CALIOP's inability to detect thin lofted aerosol layers, which can be an important source of AOD over ocean basins, and a significant contributor to the aerosol hemispheric background.

[67] However, by examining the vertical distributions, we find that even with the detection limit applied, discrepancies remain between CALIOP and GEOS-Chem aerosol extinction at low altitudes. The species classifications suggest that this is only partly due to an underestimation of pollution outflow while the majority is due to a missing source of "clean marine" aerosols in the GEOS-Chem simulation, consistent with *Lapina et al.* [2011]. We also find that while GEOS-Chem is correctly attributing the majority of AOD in the Northern Hemisphere to dust and pollution, it overestimates the strength of the dust source over North Africa and the pollution source over Asia, while underestimating a source over the southeastern U.S. and a smoke or pollution source over Southeast Asia.

[68] Although TES measures profiles of CO, its limited vertical sensitivity makes it difficult to accurately assess the model representation of vertical distributions and compare with satellite aerosol observations. However, maps of the fraction of the pollutants in the boundary layer demonstrate that while overall CO columns simulated by GEOS-Chem are biased low, the model captures the observed fraction that remains in the PBL within 5%.

[69] In this work, we investigate CO and aerosol distributions as multiyear seasonal averages and make general conclusions about transport in the Northern Hemisphere and the ability of GEOS-Chem to reproduce the spatial and vertical distribution of CO and aerosols observed from space. While we note several regions where the model and observations diverge (e.g., over Southeast Asia, Southeastern U.S., Europe, and outflow off Asia), we did not venture into examining each of these regions in great detail. Future study of these regions in the context of the analysis presented here is required to fully understand misrepresentations of emission sources, the impact of misclassification of clouds and aerosols, and differences in export mechanisms. This survey of vertical distributions demonstrates both the potential constraints offered by new satellite observations, particularly CALIOP, for tracking pollution features and also the challenges and considerations required to make useful and accurate comparisons with models.

[70] **Acknowledgments.** This work was supported by NASA (NNX08AN75G). B.F. was also partially supported by the Ball Aerospace-Colorado State University Joint Research Program. We thank the CALIOP and MODIS teams for the development and processing of the aerosol retrievals.

References

Akimoto, H. (2003), Global air quality and pollution, *Science*, *302*(5651), 1716–1719, doi:10.1126/science.1092666.

Al-Saadi, J., et al. (2005), Improving national air quality forecasts with satellite aerosol observations, *Bull. Am. Meteorol. Soc.*, *86*(9), 1249–1261, doi:10.1175/BAMS-86-9-1249.

Alexander, B., R. J. Park, D. J. Jacob, Q. B. Li, R. M. Yantosca, J. Savarino, C. C. W. Lee, and M. H. Thiemens (2005), Sulfate formation in sea-salt aerosols: Constraints from oxygen isotopes, *J. Geophys. Res.*, *110*, D10307, doi:10.1029/2004JD005659.

Ansmann, A., H. Baats, M. Tesche, D. Muller, D. Althausen, R. Engelmann, T. Pauliquevis, and P. Artaxo (2009), Dust and smoke transport from Africa to South America: Lidar profiling over Cape Verde and the Amazon rainforest, *Geophys. Res. Lett.*, *36*, L11802, doi:10.1029/2009GL037923.

Barrie, L. A., and M. J. Barrie (1990), Chemical components of lower tropospheric aerosols in the high arctic: Six years of observations, *J. Atmos. Chem.*, *11*(3), 211–226, doi:10.1007/BF00118349.

Beer, R., T. A. Glavich, and D. M. Rider (2001), Tropospheric emission spectrometer for the Earth Observing System's Aura satellite, *Appl. Opt.*, *40*(15), 2356–2367, doi:10.1364/AO.40.002356.

Benkovitz, C., M. Scholtz, J. Pacyna, L. Tarrasón, J. Dignon, E. Voldner, P. Spiro, J. Logan, and T. Graedel (1996), Global gridded inventories of anthropogenic emissions of sulfur and nitrogen, *J. Geophys. Res.*, *101*(D22), 29,239–29,253, doi:10.1029/96JD00126.

Bond, T. C., D. G. Streets, K. F. Yarber, S. M. Nelson, J.-H. Woo, and Z. Klimont (2004), A technology-based global inventory of black and organic carbon emissions from combustion, *J. Geophys. Res.*, *109*, D14203, doi:10.1029/2003JD003697.

Chin, M., T. Diehl, P. Ginoux, and W. Malm (2007), Intercontinental transport of pollution and dust aerosols: implications for regional air quality, *Atmos. Chem. Phys.*, *7*, 5501–5517, doi:10.5194/acp-7-5501-2007.

Chung, S. H., and J. H. Seinfeld (2002), Global distribution and climate forcing of carbonaceous aerosols, *J. Geophys. Res.*, *107*(D19), 4407, doi:10.1029/2001JD001397.

Cooke, W., C. Liousse, H. Cachier, and J. Feichter (1999), Construction of a 1° × 1° fossil fuel emission data set for carbonaceous aerosol and implementation and radiative impact in the ECHAM4 model, *J. Geophys. Res.*, *104*(D18), 22,137–22,162, doi:10.1029/1999JD900187.

Dacre, H. F., S. L. Gray, and S. E. Belcher (2007), A case study of boundary layer ventilation by convection and coastal processes, *J. Geophys. Res.*, *112*, D17106, doi:10.1029/2006JD007984.

Deeter, M. N., et al. (2004), Evaluation of operational radiances for the Measurements of Pollution in the Troposphere (MOPITT) instrument CO thermal band channels, *J. Geophys. Res.*, *109*, D03308, doi:10.1029/2003JD003970.

Deeter, M. N., D. P. Edwards, J. C. Gille, and J. R. Drummond (2007), Sensitivity of MOPITT observations to carbon monoxide in the lower troposphere, *J. Geophys. Res.*, *112*, D24306, doi:10.1029/2007JD008929.

Derwent, R. G., D. S. Stevenson, W. J. Collins, and C. E. Johnson (2004), Intercontinental transport and the origins of the ozone observed at surface sites in Europe, *Atmos. Environ.*, *38*(13), 1891–1901, doi:10.1016/j.atmosenv.2004.01.008.

Drury, E., D. J. Jacob, R. J. D. Spurr, J. Wang, Y. Shinozuka, B. E. Anderson, A. D. Clarke, J. Dibb, C. McNaughton, and R. Weber (2010), Synthesis of satellite (MODIS), aircraft (ICARTT), and surface (IMPROVE, EPA-AQS, AERONET) aerosol observations over eastern North America to improve MODIS aerosol retrievals and constrain surface aerosol concentrations and sources, *J. Geophys. Res.*, *115*, D14204, doi:10.1029/2009JD012629.

Dubovik, O., and M. D. King (2000), A flexible inversion algorithm for retrieval of aerosol optical properties from Sun and sky radiance measurements, *J. Geophys. Res.*, *105*, 9791–9806, doi:10.1029/2000JD900040.

Duncan, B. N., and I. Bey (2004), A modeling study of the export pathways of pollution from Europe: Seasonal and interannual variations (1987–1997), *J. Geophys. Res.*, *109*, D08301, doi:10.1029/2003JD004079.

Edwards, D. P., et al. (2004), Observations of carbon monoxide and aerosols from the Terra satellite: Northern Hemisphere variability, *J. Geophys. Res.*, *109*, D24202, doi:10.1029/2004JD004727.

Evans, M. J., and D. J. Jacob (2005), Impact of new laboratory studies of N_2O_5 hydrolysis on global model budgets of tropospheric nitrogen oxides, ozone, and OH, *Geophys. Res. Lett.*, *32*, L09813, doi:10.1029/2005GL022469.

Fairlie, D. T., D. J. Jacob, and R. J. Park (2007), The impact of transpacific transport of mineral dust in the United States, *Atmos. Environ.*, *41*(6), 1251–1266, doi:10.1016/j.atmosenv.2006.09.048.

Fehsenfeld, F. C., et al. (2006), International Consortium for Atmospheric Research on Transport and Transformation (ICARTT): North America to Europe—Overview of the 2004 summer field study, *J. Geophys. Res.*, *111*, D23S01, doi:10.1029/2006JD007829.

Fuelberg, H. E., D. L. Harrigan, and W. Sessions (2010), A meteorological overview of the ARCTAS 2008 mission, *Atmos. Chem. Phys.*, *10*(2), 817–842, doi:10.5194/acp-10-817-2010.

Generoso, S., I. Bey, M. Labonne, and F.-M. Breon (2008), Aerosol vertical distribution in dust outflow over the Atlantic: Comparisons between GEOS-Chem and Cloud-Aerosol Lidar and Infrared Satellite Observation (CALIPSO), *J. Geophys. Res.*, *113*, D24209, doi:10.1029/2008JD010154.

Goldstein, A. H., C. D. Koven, C. L. Heald, and I. Y. Fung (2009), Biogenic carbon and anthropogenic pollutants combine to form a cooling haze over the southeastern United States, *Proc. Natl. Acad. Sci. U. S. A.*, *106*(22), 8835–8840, doi:10.1073/pnas.0904128106.

Guenther, A., T. Karl, P. Harley, C. Wiedinmyer, P. I. Palmer, and C. Geron (2006), Estimates of global terrestrial isoprene emissions using MEGAN (Model of Emissions of Gases and Aerosols from Nature), *Atmos. Chem. Phys.*, *6*(11), 3181–3210, doi:10.5194/acp-6-3181-2006.

Guerova, G., I. Bey, J. L. Attié, R. V. Martin, J. Cui, and M. Sprenger (2006), Impact of transatlantic transport episodes on summertime ozone in Europe, *Atmos. Chem. Phys.*, *6*(8), 2057–2072, doi:10.5194/acp-6-2057-2006.

Heald, C. L., D. J. Jacob, D. B. A. Jones, P. I. Palmer, J. A. Logan, D. G. Streets, G. W. Sachse, J. C. Gille, R. N. Hoffman, and T. Nehrkorn (2004), Comparative inverse analysis of satellite (MOPITT) and aircraft (TRACE-P) observations to estimate Asian sources of carbon monoxide, *J. Geophys. Res.*, *109*, D23306, doi:10.1029/2004JD005185.

Heald, C. L., D. J. Jacob, R. J. Park, B. Alexander, T. D. Fairlie, R. M. Yantosca, and D. A. Chu (2006), Transpacific transport of Asian anthropogenic aerosols and its impact on surface air quality in the United States, *J. Geophys. Res.*, *111*, D14310, doi:10.1029/2005JD006847.

Hudman, R. C., et al. (2004), Ozone production in transpacific Asian pollution plumes and implications for ozone air quality in California, *J. Geophys. Res.*, *109*, D23S10, doi:10.1029/2004JD004974.

Hudman, R. C., et al. (2007), Surface and lightning sources of nitrogen oxides over the United States: Magnitudes, chemical evolution, and outflow, *J. Geophys. Res.*, *112*, D12S05, doi:10.1029/2006JD007912.

Hudman, R. C., L. T. Murray, D. J. Jacob, D. B. Millet, S. Turquety, S. Wu, D. R. Blake, A. H. Goldstein, J. Holloway, and G. W. Sachse (2008), Biogenic versus anthropogenic sources of CO in the United States, *Geophys. Res. Lett.*, *35*, L04801, doi:10.1029/2007GL032393.

Hunt, W. H., D. M. Winker, M. A. Vaughan, K. A. Powell, P. L. Lucker, and C. Weimer (2009), CALIPSO lidar description and performance assessment, *J. Atmos. Oceanic Technol.*, *26*(7), 1214–1228, doi:10.1175/2009JTECHA1223.1.

Jacobson, M. Z. (1998), Studying the effects of aerosols on vertical photolysis rate coefficient and temperature profiles over an urban airshed, *J. Geophys. Res.*, *103*(D9), 10,593–10,604, doi:10.1029/98JD00287.

Jaeglé, L., P. K. Quinn, T. Bates, B. Alexander, and J.-T. Lin (2011), Global distribution of sea salt aerosols: New constraints from in situ and remote sensing observations, *Atmos. Chem. Phys.*, *11*, 3137–3157.

Jaffe, D., et al. (1999), Transport of Asian air pollution to North America, *Geophys. Res. Lett.*, *26*(6), 711–714, doi:10.1029/1999GL900100.

Jordan, N. S., R. M. Hoff, and J. T. Bacmeister (2010), Validation of Goddard Earth Observing System-version 5 MERRA planetary boundary layer heights using CALIPSO, *J. Geophys. Res.*, *115*, D24218, doi:10.1029/2009JD013777.

Kaufman, Y., D. Tanreacute, L. Remer, E. Vermote, A. Chu, and B. Holben (1997), Operational remote sensing of tropospheric aerosol over land from EOS moderate resolution imaging spectroradiometer, *J. Geophys. Res.*, *102*(D14), 17,051–17,067, doi:10.1029/96JD03988.

Keating, T. J., and A. Zuber (2007), Hemispheric transport of air pollution 2007, report, U. N., New York.

Kittaka, C., D. M. Winker, M. A. Vaughan, A. Omar, and L. A. Remer (2010), Intercomparison of CALIOP and MODIS aerosol optical depth retrievals, *Atmos. Meas. Tech. Discuss.*, *3*(4), 3319–3344, doi:10.5194/amtd-3-3319-2010.

Kopacz, M., et al. (2010), Global estimates of CO sources with high resolution by adjoint inversion of multiple satellite datasets (MOPITT, AIRS, SCIAMACHY, TES), *Atmos. Chem. Phys.*, *10*(3), 855–876, doi:10.5194/acp-10-855-2010.

Kuhns, H., M. Green, and V. Etyemezian (2003), Big Bend Regional Aerosol and Visibility Observational (BRAVO) study emissions inventory, report, Desert Res. Inst., Las Vegas, Nev.

Lapina, K., et al. (2011), Investigating organic aerosol loading in the remote marine environment, *Atmos. Chem. Phys.*, *11*, 8847–8860, doi:10.5194/acp-11-8847-2011.

Levy, H. I., and W. J. Moxim (1989), Simulated global distribution and deposition of reactive nitrogen emitted by fossil fuel combustion, *Tellus, Ser. B*, *41*, 256–271, doi:10.1111/j.1600-0889.1989.tb00305.x.

Levy, R. C., L. A. Remer, J. V. Martins, Y. J. Kaufman, A. Plana-Fattori, J. Redemann, and B. Wenny (2005), Evaluation of the MODIS aerosol retrievals over ocean and land during CLAMS, *J. Atmos. Sci.*, *62*(4), 974–992, doi:10.1175/JAS3391.1.

Levy, R. C., L. A. Remer, R. G. Kleidman, S. Mattoo, C. Ichoku, R. Kahn, and T. F. Eck (2010), Global evaluation of the collection 5 MODIS aerosol products over land and ocean, *Atmos. Chem. Phys. Discuss.*, *10*, 14,815–14,873, doi:10.5194/acpd-10-14815-2010.

Li, Q., et al. (2002), Transatlantic transport of pollution and its effects on surface ozone in Europe and North America, *J. Geophys. Res.*, *107*(D13), 4166, doi:10.1029/2001JD001422.

Li, Q., D. J. Jacob, R. Park, Y. Wang, C. L. Heald, R. Hudman, R. M. Yantosca, R. V. Martin, and M. Evans (2005), North American pollution outflow and the trapping of convectively lifted pollution by upper-level anticyclone, *J. Geophys. Res.*, *110*, D10301, doi:10.1029/2004JD005039.

Liao, H., Y. L. Yung, and J. H. Seinfeld (1999), Effects of aerosols on tropospheric photolysis rates in clear and cloudy atmospheres, *J. Geophys. Res.*, *104*(D19), 23,697–23,707, doi:10.1029/1999JD900409.

Liao, H., D. K. Henze, J. H. Seinfeld, S. Wu, and L. J. Mickley (2007), Biogenic secondary organic aerosol over the United States: Comparison of climatological simulations with observations, *J. Geophys. Res.*, *112*, D06201, doi:10.1029/2006JD007813.

Lin, J.-T., and M. B. McElroy (2010), Impacts of boundary layer mixing on pollutant vertical profiles in the lower troposphere: Implications to satellite remote sensing, *Atmos. Environ.*, *44*, 1726–1739, doi:10.1016/j.atmosenv.2010.02.009.

Lin, J.-T., D. Youn, X.-Z. Liang, and D. J. Wuebbles (2008), Global model simulation of summertime U.S. ozone diurnal cycle and its sensitivity to PBL mixing, spatial resolution, and emissions, *Atmos. Environ.*, *42*(36), 8470–8483, doi:10.1016/j.atmosenv.2008.08.012.

Liu, H., D. Jacob, I. Bey, and R. Yantosca (2001), Constraints from ^{210}Pb and ^{7}Be on wet deposition and transport in a global three-dimensional chemical tracer model driven by assimilated meteorological fields, *J. Geophys. Res.*, *106*(D11), 12,109–12,128, doi:10.1029/2000JD900839.

Liu, H., D. J. Jacob, I. Bey, R. M. Yantosca, and B. N. Duncan (2003), Transport pathways for Asian pollution outflow over the Pacific: Interannual and seasonal variations, *J. Geophys. Res.*, *108*(D20), 8786, doi:10.1029/2002JD003102.

Liu, J., D. L. Mauzerall, L. W. Horowitz, P. Ginoux, and A. M. Fiore (2009), Evaluating inter-continental transport of fine aerosols: (1) Methodology, global aerosol distribution and optical depth, *Atmos. Environ.*, *43*(28), 4327–4338, doi:10.1016/j.atmosenv.2009.03.054.

Liu, Z., M. A. Vaughan, D. M. Winker, C. A. Hostetler, L. R. Poole, D. Hlavka, W. Hart, and M. McGill (2004), Use of probability distribution functions for discriminating between cloud and aerosol in lidar backscatter data, *J. Geophys. Res.*, *109*, D15202, doi:10.1029/2004JD004732.

Lopez, J. P., M. Luo, L. E. Christensen, M. Loewenstein, H. Jost, C. R. Webster, and G. Osterman (2008), TES carbon monoxide validation during two AVE campaigns using the Argus and ALIAS instruments on NASA's WB-57F, *J. Geophys. Res.*, *113*, D16S47, doi:10.1029/2007JD008811.

Luo, M., et al. (2007a), TES carbon monoxide validation with DACOM aircraft measurements during INTEX-B 2006, *J. Geophys. Res.*, *112*, D24S48, doi:10.1029/2007JD008803.

Luo, M., et al. (2007b), Comparison of carbon monoxide measurements by TES and MOPITT: Influence of a priori data and instrument characteristics on nadir atmospheric species retrievals, *J. Geophys. Res.*, *112*, D09303, doi:10.1029/2006JD007663.

Martin, R. V., D. J. Jacob, R. M. Yantosca, M. Chin, and P. Ginoux (2003), Global and regional decreases in tropospheric oxidants from photochemical effects of aerosols, *J. Geophys. Res.*, *108*(D3), 4097, doi:10.1029/2002JD002622.

Mielonen, T., A. Arola, M. Komppula, J. Kukkonen, J. Koskinen, G. de Leeuw, and K. E. J. Lehtinen (2009), Comparison of CALIOP level 2 aerosol subtypes to aerosol types derived from AERONET inversion data, *Geophys. Res. Lett.*, *36*, L18804, doi:10.1029/2009GL039609.

Olivier, J. G. J., and J. J. M. Berdowski (2001), Global emissions sources and sinks, in *The Climate System*, edited by J. Berdowski, R. Guicherit, and B. J. Heij, pp. 33–78, A. A. Balkema, Lisse, Netherlands.

Olivier, J. G. J., J. J. M. Berdowski, J. A. H. W. Peters, J. Bakker, A. J. H. Visschedijk, and J.-P. J. Bloos (2001), Applications of EDGAR. Including a description of EDGAR 3.0: Reference database with trend data for 1970–1995, *Rep. 773301001*, 142 pp., Rijksinst. Voor Volksgezond. en Milieu, Bilthoven, Netherlands.

Omar, A. H., D. M. Winker, M. A. Vaughan, Y. Hu, C. R. Trepte, R. A. Ferrare, K.-P. Lee, and C. A. Hostetler (2009), The CALIPSO automated aerosol classification and lidar ratio selection algorithm, *J. Atmos. Oceanic Technol.*, *26*, 1994–2014, doi:10.1175/2009JTECHA1231.1.

Oo, M., and R. Holz (2011), Improving the CALIOP aerosol optical depth using combined MODIS-CALIOP observations and CALIOP integrated attenuated total color ratio, *J. Geophys. Res.*, *116*, D14201, doi:10.1029/2010JD014894.

Osterman, G. (2007), Tropospheric Emission Spectrometer (TES) validation report version F04_04 DataRep, Jet Propul. Lab., Pasadena, Calif.

Owen, R. C., O. R. Cooper, A. Stohl, and R. E. Honrath (2006), An analysis of the mechanisms of North American pollutant transport to the central North Atlantic lower free troposphere, *J. Geophys. Res.*, *111*, D23S58, doi:10.1029/2006JD007062.

Park, R. J., D. J. Jacob, M. Chin, and R. V. Martin (2003), Sources of carbonaceous aerosols over the United States and implications for natural visibility, *J. Geophys. Res.*, *108*(D12), 4355, doi:10.1029/2002JD003190.

Park, R. J., D. J. Jacob, B. D. Field, R. M. Yantosca, and M. Chin (2004), Natural and transboundary pollution influences on sulfate-nitrate-ammonium aerosols in the United States: Implications for policy, *J. Geophys. Res.*, *109*, D15204, doi:10.1029/2003JD004473.

Parrington, M., D. B. A. Jones, K. W. Bowman, L. W. Horowitz, A. M. Thompson, D. W. Tarasick, and J. C. Witte (2008), Estimating the summertime tropospheric ozone distribution over North America through assimilation of observations from the Tropospheric Emission Spectrometer, *J. Geophys. Res.*, *113*, D18307, doi:10.1029/2007JD009341.

Parrish, D. D., et al. (2009), Overview of the Second Texas Air Quality Study (TexAQS II) and the Gulf of Mexico Atmospheric Composition and Climate Study (GoMACCS), *J. Geophys. Res.*, *114*, D00F13, doi:10.1029/2009JD011842. [Printed *115*(D7), 2010.]

Perry, K. D., T. A. Cahill, R. C. Schnell, and J. M. Harris (1999), Long-range transport of anthropogenic aerosols to the National Oceanic and Atmospheric Administration baseline station at Mauna Loa Observatory, Hawaii, *J. Geophys. Res.*, *104*(D15), 18,521–18,533, doi:10.1029/1998JD100083.

Price, H. U., D. A. Jaffe, O. R. Cooper, and P. V. Doskey (2004), Photochemistry, ozone production, and dilution during long-range transport episodes from Eurasia to the northwest United States, *J. Geophys. Res.*, *109*, D23S13, doi:10.1029/2003JD004400.

Prospero, J. (1981), Aeolian transport to the world ocean, in *The Oceanic Lithosphere*, edited by C. Emiliani, pp. 801–874, John Wiley, New York.

Prospero, J. (1999), Long-term measurements of the transport of African mineral dust to the southeastern United States: Implications for regional air quality, *J. Geophys. Res.*, *104*(D13), 15,917–15,927, doi:10.1029/1999JD900072.

Quinn, P. K., G. Shaw, E. Andrews, E. G. Dutton, T. Ruoho-Airola, and S. L. Gong (2007), Arctic haze: Current trends and knowledge gaps, *Tellus, Ser. B*, *59*(1), 99–114, doi:10.1111/j.1600-0889.2006.00238.x.

Redemann, J., M. A. Vaughan, Q. Zhang, Y. Shinozuka, P. B. Russell, J. M. Livingston, M. Kacenelenbogen, and L. A. Remer (2011), The comparison of MODIS-Aqua (C5) and CALIOP (V2 & V3) aerosol optical depth, *Atmos. Chem. Phys. Discuss.*, *11*(8), 22,987–23,027, doi:10.5194/acpd-11-22987-2011.

Reidmiller, D. R., D. A. Jaffe, D. Chand, S. Strode, P. Swartzendruber, G. M. Wolfe, and J. A. Thornton (2009), Interannual variability of long-range transport as seen at the Mt. Bachelor observatory, *Atmos. Chem. Phys.*, *9*(2), 557–572, doi:10.5194/acp-9-557-2009.

Remer, L. A., et al. (2005), The MODIS aerosol algorithm, products, and validation, *J. Atmos. Sci.*, *62*(4), 947–973, doi:10.1175/JAS3385.1.

Remer, L. A., et al. (2008), Global aerosol climatology from the MODIS satellite sensors, *J. Geophys. Res.*, *113*, D14S07, doi:10.1029/2007JD009661

Ridley, D. R., C. L. Heald, and B. Ford (2012), North African dust export and deposition: A satellite and model perspective, *J. Geophys. Res.*, *117*, D02202, doi:10.1029/2011JD016794.

Rodgers, C. D. (2000), *Inverse Methods for Atmospheric Sounding: Theory and Practice*, 240 pp., World Sci., Hackensack, N.

Sayer, A. M., A. Smirnov, C. Hsu, and B. N. Holben (2012), A pure marine aerosol model, for use in remote sensing applications, *J. Geophys. Res.*, doi:10.1029/2011JD016689, in press.

Singh, H. B., W. H. Brune, J. H. Crawford, D. J. Jacob, and P. B. Russell (2006), Overview of the summer 2004 Intercontinental Chemical Transport Experiment–North America (INTEX-A), *J. Geophys. Res.*, *111*, D24S01, doi:10.1029/2006JD007905.

Stohl, A., and S. Eckhardt (2004), Intercontinental transport of air pollution: An introduction, in *Air Pollution*, edited by A. Stohl, pp. 1–11, Springer, Berlin.

Stohl, A., S. Eckhardt, C. Forster, P. James, and N. Spichtinger (2002), On the pathways and timescales of intercontinental air pollution transport, *J. Geophys. Res.*, *107*(D23), 4684, doi:10.1029/2001JD001396.

van der Werf, G. R., J. T. Randerson, L. Giglio, G. J. Collatz, P. S. Kasibhatla, and A. F. Arellano Jr. (2006), Interannual variability in global biomass burning emissions from 1997 to 2004, *Atmos. Chem. Phys.*, *6*(11), 3423–3441, doi:10.5194/acp-6-3423-2006.

van Donkelaar, A., R. V. Martin, M. Brauer, R. Kahn, R. Levy, C. Verduzco, and P. J. Villeneuve (2010), Global estimates of ambient fine particulate matter concentrations from satellite-based aerosol optical depth: Development and application, *Environ. Health Perspect.*, *118*(6), 847–855 doi:10.1289/ehp.0901623.

Vaughan, M., S. Young, D. Winker, K. Powell, A. Omar, Z. Liu, Y. Hu, and C. Hostetler (2004), Fully automated analysis of space-based lidar data: an overview of the CALIPSO retrieval algorithms and data products, *Proc. SPIE*, *5575*, 16–30, doi:10.1117/12.572024.

Vestreng, V., K. Mareckova, S. Kakareka, A. Malchykhina, and T. Kukharchyk (2007), Inventory review 2007; emission data reported to LRTAP Convention and NEC Directive, *MSC-W Tech. Rep. 1/07Rep.*, Norw. Meteorol. Inst., Oslo.

Wang, Y. H., D. J. Jacob, and J. A. Logan (1998), Global simulation of tropospheric O_3-NO_x-hydrocarbon chemistry: 3. Origin of tropospheric ozone and effects of nonmethane hydrocarbons, *J. Geophys. Res.*, *103*(D9), 10,757–10,767, doi:10.1029/98JD00156.

Wesely, M. L. (1989), Parameterization of surface resistances to gaseous dry deposition in regional-scale numerical models, *Atmos. Environ.*, *23*(6), 1293–1304.

Winker, D. M., J. R. Pelon, and M. P. McCormick (2003), The CALIPSO mission: Spaceborne lidar for observation of aerosols and clouds, paper presented at Lidar Remote Sensing for Industry and Environment Monitoring III, SPIE – Int. Soc. for Opt. Eng., Hangzhou, China.

Winker, D. M., M. A. Vaughan, A. Omar, Y. Hu, K. A. Powell, Z. Liu, W. H. Hunt, and S. A. Young (2009), Overview of the CALIPSO mission and CALIOP data processing algorithms, *J. Atmos. Oceanic Technol.*, *26*, 2310–2323, doi:10.1175/2009JTECHA1281.1.

Winker, D. M., et al. (2010), The CALIPSO mission: A global 3D view of aerosols and clouds, *Bull. Am. Meteorol. Soc.*, *91*(9), 1211–1229, doi:10.1175/2010BAMS3009.1.

Yevich, R., and J. A. Logan (2003), An assessment of biofuel use and burning of agricultural waste in the developing world, *Global Biogeochem. Cycles*, *17*(4), 1095, doi:10.1029/2002GB001952.

Yu, H., L. A. Remer, M. Chin, H. Bian, R. G. Kleidman, and T. Diehl (2008), A satellite-based assessment of transpacific transport of pollution aerosol, *J. Geophys. Res.*, *113*, D14S12, doi:10.1029/2007JD009349.

Yu, H., M. Chin, D. M. Winker, A. H. Omar, Z. Liu, C. Kittaka, and T. Diehl (2010), Global view of aerosol vertical distributions from CALIPSO lidar measurements and GOCART simulations: Regional and seasonal variations, *J. Geophys. Res.*, *115*, D00H30, doi:10.1029/2009JD013364.

Zhang, J., and J. S. Reid (2006), MODIS aerosol product analysis for data assimilation: Assessment of over-ocean level 2 aerosol optical thickness retrievals, *J. Geophys. Res.*, *111*, D22207, doi:10.1029/2005JD006898.

Zhang, L., et al. (2008), Transpacific transport of ozone pollution and the effect of recent Asian emission increases on air quality in North America: An integrated analysis using satellite, aircraft, ozonesonde, and surface observations, *Atmos. Chem. Phys.*, *8*, 6117–6136, doi:10.5194/acp-8-6117-2008.

Zhang, Q., et al. (2009), Asian emissions in 2006 for the NASA INTEX-B mission, *Atmos. Chem. Phys.*, *9*, 5131–5153, doi:10.5194/acp-9-5131-2009.

B. Ford, Department of Atmospheric Science, Colorado State University, Fort Collins, CO 80523-1371, USA. (bonne@atmos.colostate.edu)

C. L. Heald, Department of Civil and Environmental Engineering, MIT, Cambridge, MA 02139, USA.